Title

Trajectory-based modeling of fluid transport in a medium with smoothly varying heterogeneity

Journal

Water Resources Research, 52(4)

ISSN

0043-1397

Authors

Vasco, DW
Pride, Steven R
Commer, Michael

Publication Date

2016-04-01

DOI

10.1002/2015wr017646

Peer reviewed

AGU PUBLICATIONS

Water Resources Research

RESEARCH ARTICLE
10.1002/2015WR017646

Key Points:
- A semianalytic solution for tracer transport is introduced
- A fully general dispersion tensor and smoothly varying heterogeneity are included in the model
- The approach forms the basis for an efficient imaging or inversion algorithm

Correspondence to:
D. W. Vasco,
dwvasco@lbl.gov

Citation:
Vasco, D. W., S. R. Pride, and M. Commer (2016), Trajectory-based modeling of fluid transport in a medium with smoothly varying heterogeneity, *Water Resour. Res.*, *52*, 2618–2646, doi:10.1002/2015WR017646.

Received 1 JUN 2015
Accepted 26 FEB 2016
Accepted article online 4 MAR 2016
Published online 4 APR 2016

Trajectory-based modeling of fluid transport in a medium with smoothly varying heterogeneity

D. W. Vasco[1], Steven R. Pride[1], and Michael Commer[1]

[1]Energy Geosciences Division, Lawrence Berkeley National Laboratory, University of California, Berkeley, California, USA

Abstract Using an asymptotic methodology, valid in the presence of smoothly varying heterogeneity and prescribed boundaries, we derive a trajectory-based solution for tracer transport. The analysis produces a Hamilton-Jacobi partial differential equation for the phase of the propagating tracer front. The trajectories follow from the characteristic equations that are equivalent to the Hamilton-Jacobi equation. The paths are determined by the fluid velocity field, the total porosity, and the dispersion tensor. Due to their dependence upon the local hydrodynamic dispersion, they differ from conventional streamlines. This difference is borne out in numerical calculations for both uniform and dipole flow fields. In an application to the computational X-ray imaging of a saline tracer test, we illustrate that the trajectories may serve as the basis for a form of tracer tomography. In particular, we use the onset time of a change in attenuation for each volume element of the X-ray image as a measure of the arrival time of the saline tracer. The arrival times are used to image the spatial variation of the effective hydraulic conductivity within the laboratory sample.

1. Introduction

A range of numerical reservoir simulators are now available for modeling flow and transport. For example, there are finite difference, finite-element algorithms, and finite-volume approaches. Given sufficient attention to the numerics of the problem, purely numerical flow simulators can generally provide accurate solutions to the equations governing flow and transport. However, due to the complexity of many current simulation efforts, there is a need for semianalytic descriptions of flow and transport that can be of use in interpreting the results of both numerical simulation and experiments. For example, an analytical solution can provide a clear relationship between medium properties and features associated with a break-through curve, such as the arrival time of a pulse. Such relationships are particularly valuable when treating the inverse problem in which the observations are used to infer properties of the medium. To be useful, the semianalytic solutions must be valid for realistic media. It is important for such descriptions to be valid in two and three-dimensional settings and in the presence of substantial heterogeneity.

There are a number of analytic and semianalytic methods for modeling transport but such techniques are typically restricted to structured porous media. Several analytic solutions are discussed in the report of *van Genuchten and Alves* [1982] and the book by *Javandel et al.* [1984], including the work of *Cleary and Ungs* [1978]. Such purely analytic solutions generally require a homogeneous whole-space structure. Using the method of images, whole space solutions may be extended to a semi-infinite half-space and a single uniform layer, as in the analytic Green's function solution of *Park and Zhan* [2001]. Other analytic approaches assume special forms for the flow field and the dispersion or diffusion, such as linear distance dependent dispersion [*Chen et al.*, 2008], diffusion proportional to the square of the velocity [*Zoppou and Knight*, 1999], dispersivity with a power-law dependence in the similarity solution of *Su et al.* [2005], and a segmented linear diffusion coefficient for the orthogonal expansion technique developed by *Liu and Si* [2008]. Transform methods, applicable to porous media with properties that are uniform or vary in one dimension, have been used to produce a variety of semianalytic solutions. These include the direct application of the Laplace transform [*Yates*, 1990; *Xu and Brusseau*, 1996; *Shan and Javandel*, 1997; *Sim and Chrysikopoulos*, 1999; *Moridis*, 2002] as well as extensions, such as the generalized integral transform technique (GITT) [*Mikhailov and Özisik*, 1984; *Cotta*, 1992; *Cotta and Mikhailov*, 1993; *Guerrero and Skaggs*, 2010]. There are also asymptotic methods for layered media [*Gelhar and Collins*, 1971].

Streamline simulation is a semianalytic technique that is valid in three-dimensional heterogeneous porous media [*Datta-Gupta and King*, 1995; *Blunt et al*., 1996; *Bratvedt et al*., 1996; *Cirpka et al*., 1999a]. Streamline methods have increased in sophistication and are used in high-resolution reservoir models [*Datta-Gupta and King*, 2007]. Streamline methods are now used to model reactive transport involving multiple components [*Yabusaki et al*., 1998; *Cirpka et al*., 1999b]. However, streamline methods typically neglect dispersion in their formulation and must implement it using an additional technique, such as operator splitting [*Datta-Gupta and King*, 2007]. Thus, the paths are not influenced by the dispersion and are less helpful in visualizing the physical tracer movement and in understanding those factors contributing to the motion.

In this paper, we present an alternative asymptotic formulation for modeling tracer transport including a generally anisotropic dispersion tensor and smoothly varying, but otherwise arbitrary, heterogeneity. Thus, the approach is not limited to structured or symmetric porous media. The approach produces an expression for the motion of the transported material that is influenced by the dispersion matrix **D**, the flow field **q**, and the total porosity φ_k. This contrasts with a streamline that is computed using only the flow field and the porosity. The equations governing the construction of the trajectories provide insight into the factors controlling tracer transport that include the flow field, the porosity, and the dispersion tensor. Due to the presence of the dispersion tensor, there is an additional term in the differential equation for the trajectory, determining the deviation of the path from a conventional streamline. As we shall see, factors such as molecular diffusion, the flow velocity, and longitudinal and transverse dispersion, all impact the path of the dissolved species concentration. Asymptotic techniques, similar to those discussed in this paper, have been used in the study of convection-diffusion [*Smith*, 1981; *Knessl and Keller*, 1997; *Chapman et al*., 1999; *Vasco and Datta-Gupta*, 1999]. However, these approaches did not include a general dispersion matrix. Multiple-scale asymptotic approaches have also been used to compute the macroscopic tracer concentration from pore and subpore flow, a technique known as homogenization [*Hornung*, 1997; *Attinger et al*., 2001]. Those approaches typically seek to average the smaller scale structure in permeability and flow variations into effective properties to simplify the modeling. Such solutions are distinct from ours, as we are allowing for the effects of larger-scale heterogeneity in both permeability and dispersion in our model.

The asymptotic method presented here is a tool which may be the basis of efficient imaging algorithms. As shown in our application below, using the technique one can devise a strategy in which a single simulation is all that is required for one step in the inverse modeling of tracer observations [*Vasco and Datta-Gupta*, 1999; *Datta-Gupta et al*., 2002]. The trajectory-based inversion algorithm scales well with the size of the reservoir model, growing in a linear fashion with the number of grid blocks intersected by the path. The assumptions upon which the approach is based, smoothly-varying properties within the boundaries of the model, are compatible with our use of the technique in inverse modeling. Often, due to inherent limitations in resolution and regularization, the model updates are relatively smooth in comparison to the tracer front.

2. Methodology

An outline of the trajectory-based approach is provided in this section. First, we present the equation governing transport in the subsurface.

2.1. Governing Equation

The equation governing transport of an inert solute in a dispersive medium is [*Bear*, 1972; *de Marsily*, 1986, p. 240]

$$\nabla \cdot (\mathbf{D} \cdot \nabla c - \mathbf{q}c) = \varphi_k \frac{\partial c}{\partial t} \tag{1}$$

where $c(\mathbf{x}, t)$ is the dissolved species concentration within the fluid, in units of ML^{-3}, φ_k is the total porosity, **D** is the dispersion tensor. The dispersion tensor represents the effects of small-scale flow heterogeneity. That is, heterogeneity varying over a length scale that is less than the dimensions of the grid blocks or the nodal spacings used in numerical representations of the spatial variations in flow properties. The effect of larger-scale heterogeneity is represented by the macroscopic variations contained within the reservoir model. The vector **q** is the Darcy velocity, given by

$$\mathbf{q} = -\mathbf{K} \cdot \nabla h, \tag{2}$$

where **K** (**x**) is the hydraulic conductivity tensor and $h(\mathbf{x}, t)$ is the hydraulic head. The hydrodynamic dispersion of a solute encompasses the spreading of the material due to the local heterogeneity of both the

porous material as well as the flow field. The earliest studies emphasized both diffusion and the mixing due to variable velocity for flow in small tubes [*Taylor*, 1953, 1954]. One early examination of the small-scale mixing caused by flow variation in a microscopically heterogeneous porous medium was by *Scheidegger* [1954]. Following this early work, it was realized that dispersion is inherently anisotropic, even in an isotropic medium, with principle directions determined by the flow direction [*de Josselin de Jong*, 1958; *Saffman*, 1959; *Nikolaevskii*, 1959; *Bear*, 1961; *Scheidegger*, 1961]. Our understanding of transport in heterogeneous permeable media has advanced due to the contributions of stochastic methods to hydrology [*Warren and Skiba*, 1964; *Schwartz*, 1977; *Gelhar et al*., 1979; *Dagan*, 1982; *Gelhar and Axness*, 1983]. As a result of these and other efforts, there are now several models of dispersion in a porous medium, each limited in some respect [*Sahimi*, 1993], and work in this area continues [*Bruining et al*., 2012; *Liu and Kitanidis*, 2013]. Here we adopt a fairly established approach that accounts for both molecular diffusion and hydrodynamic dispersion. Experimental evidence, such as that cited by *De Marsily* [1986, p. 237], indicates that in most flow regimes and for an isotropic medium, the dispersion along (D_l) and transverse (D_t) to the flow direction, are well approximated by the general forms

$$D_l = \varphi_k d_m + \alpha_l q \tag{3}$$

and

$$D_t = \varphi_k d_m + \alpha_t q \tag{4}$$

where d_m is the molecular diffusion coefficient, q is the magnitude of the Darcy velocity vector. The parameters α_l and α_t are the intrinsic dispersion coefficients, or dispersivities, in the longitudinal and transverse directions (with respect to the flow direction). The form of the coefficient has been generalized to allow for transverse anisotropic media [*Fel and Bear*, 2010]. The approach described below is appropriate for a general anisotropic porous medium in which the dispersion in the principle directions of the dispersion tensor are given by three scalars, say D_1, D_2, and D_3. Hence, our development will be in terms of a general tensor **D**.

Commonly, the dispersion tensor is assumed to be symmetric. However, the symmetry of the dispersion tensor has been called into question [*Carbonell and Whitaker*, 1983; *Koch and Brady*, 1987; *Didierjean et al*., 1997; *Auriault et al*., 2010]. The asymmetry of the dispersion tensor, demonstrated by *Koch and Brady* [1987], was recently verified by *Auriault et al*. [2010] in the case of low Peclet numbers. As noted by *Carbonell and Whitaker* [1983], in a uniform medium only the symmetric component of the dispersion tensor influences the transport. This is easily seen by considering equation (1) when the dispersion tensor does not depend upon position. The symmetry of the array of second-order spatial derivatives of C, and the invariance of the other terms in the equation, implies the symmetry of the dispersion tensor. Perhaps because this symmetry holds in homogeneous media, but does not carry over to heterogeneous media, the general asymmetry of **D** has not been emphasized in hydrology. In the discussion that follows, we will develop a solution that does not require **D** to be a symmetric matrix.

2.1.1. Transformation Into the Frequency Domain

Because the primary application that we have in mind is a tracer test conducted under the condition of steady-state flow, the pressure field will not change as a function of time. Therefore, the coefficients **D**, **q**, and φ_k do not depend upon time and one may apply an integral transform to remove the time derivative. Here we consider the Fourier transform [*Bracewell*, 1978] of the concentration $c(\mathbf{x}, t)$, resulting in a function $C(\mathbf{x}, \omega)$ that depends upon frequency ω. Transforming equation (1), using the properties of the Fourier transform gives

$$\nabla \cdot (\mathbf{D} \cdot \nabla C - \mathbf{q}C) + i\omega\varphi_k C = 0, \tag{5}$$

an equation that only contains spatial derivatives. Note that the technique used to generate the semianalytic solution, the method of multiple scales, can also be applied in the time-domain. Therefore, the assumption of time-invariant flow is not necessary in order to apply this technique and a more general solution can be developed in the time domain.

2.2. A Trajectory-Based Solution for Dispersive Transport

For a general model, equation (1) is usually solved numerically, using a method such as finite-differences, integral finite-differences [*Pruess et al*., 1999], finite-elements, particle tracking, or lattice-

Boltzmann [*Flekkoy*, 1993]. However, for a medium in which the properties vary smoothly between known boundaries, one can obtain useful semianalytic solutions using asymptotic techniques. By smoothly varying, we mean that the spatial variation in material properties is smoother than the spatial variation across the concentration front. A quantitative expression of smoothness is provided by the ratio of the length scales of these variations. That is, let L represent the length scale associated with the variation in flow properties and l represent the length scale corresponding to variations across the concentration front. We assume that $L \gg l$ and hence, the ratio

$$\epsilon = l/L,$$

known as the scale factor, is much less than 1. The method should be sufficiently accurate when the length scale of the heterogeneity is greater than the width of the transition zone across the tracer front. Some examples of such transition zones are provided in the figures that follow. The method should have difficulties with heterogeneity that varies more rapidly than the width of the transition zone, for example at a sharp interface between layers. In the manner of asymptotic ray theory [*Kline and Kay*, 1979; *Chapman*, 2004], it is possible to account for such sharp interfaces as explicit boundary conditions.

It is instructive to examine the limit as ϵ approaches very small values. An extreme example is provided by an infinite, homogeneous medium, in which case the length scale of the heterogeneity is effectively infinite and the ratio ϵ approaches zero. An alternative way for ϵ to take on small values is for the front to become very steep or very sharp. In this limit, the leading edge of the front becomes sharp and approaches either a step or delta function, depending on the variation of the injection rate with time (constant rate or injection pulse). We discuss the case of a rapid variation in concentration below and show that the asymptotic solution is essentially identical to the analytic solution. In these cases, as we shall see below, the power series used to represent the solution reduces to the zeroth-order term. This term produces a generalization of the analytic solution for a homogeneous medium, where the parameters of the solution are now functions accounting for the smoothly varying heterogeneity.

Note that the asymptotic approach, based upon the two scales l and L, is formally equivalent to the method of homogenization that is often used to derive a larger-scale effective medium from smaller-scale structure [*Hornung*, 1997; *Attinger et al*., 2001]. In fact, the mechanics of the approaches are identical in many respects. However, our aim in this work is different from that of homogenization. We wish to derive approximate and revealing solutions that reflect the influence of the large-scale heterogeneous structure and yet are not much more complicated than are analytic solutions associated with a homogeneous medium. This desire follows from our goal of developing tools that can be used for the efficient and flexible solution of the inverse problem, in which we estimate medium properties from observations.

An asymptotic solution is a representation of the concentration in terms of a power series in the scale parameter ϵ

$$C(\mathbf{x}, \omega, \theta) = e^{\theta(\mathbf{x},\omega)} \sum_{n=0}^{\infty} \epsilon^n C_n(\mathbf{x}, \omega), \tag{6}$$

where $\theta(\mathbf{x}, \omega)$ is the phase, a quantity associated with the propagation of the tracer front. The terms $C_n(\mathbf{x}, \omega)$ represent amplitude adjustments of various orders in ϵ. One advantage of this form of the solution in equation (6) is that only the first few terms of the expansion are important when $\epsilon \ll 1$. The partitioned form of the solution into phase and amplitude terms is also advantageous. This partitioning provides flexibility in forward and inverse modeling, allowing for techniques such as tracer arrival time tomography [*Vasco and Datta-Gupta*, 1999; *Datta-Gupta et al*., 2002; *Vasco and Finsterle*, 2004] that we shall use in the application below.

In Appendix A, we provide the details of the asymptotic methodology. In general, the approach involves writing the governing equation (5) in terms of new coordinates, $\mathbf{X}$, that are related to the physical coordinates through the ratio ϵ,

$$\mathbf{X} = \epsilon \mathbf{x}. \tag{7}$$

In order to do this, one rewrites all of the derivatives with respect to the physical coordinates in terms of the derivatives with respect to the $\mathbf{X}$ coordinates. Furthermore, the presence of the phase function must be

taken into account as an implicit functional dependence. In Appendix A, we write the governing equation (5) in terms of **X** and substituting in the power series expansion (6). The result is an expression containing an infinite series of terms in powers of ϵ. Because $\epsilon \ll 1$, only terms of low order in ϵ are of interest. Thus, for example, we consider terms of order $\epsilon^0 \sim 1$ in the next subsection.

2.2.1. Terms of Order $\epsilon^0 \sim 1$: An Equation for the Phase

The terms of zeroth-order in ϵ produce a first-order nonlinear partial differential equation for the phase $\theta(\mathbf{x}, \omega)$ (see equation (A9))

$$\nabla\theta \cdot \mathbf{D} \cdot \nabla\theta - \mathbf{q} \cdot \nabla\theta + i\omega\varphi_k = 0. \tag{8}$$

Equation (8) is an example of a Hamilton-Jacobi equation [*Sneddon*, 2006, p. 81], a class of equations that have proven very important in physics and applied mathematics [*Courant and Hilbert*, 1962, p. 118]. Defining the phase gradient vector

$$\mathbf{p} = \nabla\theta, \tag{9}$$

one may write equation (8) more compactly as

$$\mathbf{p} \cdot \mathbf{D} \cdot \mathbf{p} - \mathbf{q} \cdot \mathbf{p} + i\omega\varphi_k = 0. \tag{10}$$

One can solve equation (10) using the method of characteristics, developed for first-order partial differential equations [*Courant and Hilbert*, 1962, p. 62; *Sneddon*, 2006, p. 61]. This approach is discussed in Appendix B in the context of Hamilton-Jacobi theory [*Courant and Hilbert*, 1962, p. 103; *Sneddon*, 2006, p. 81]. Essentially, the independent variables **x** and **p** are considered to be functions of a scalar variable *s*. One may think of **x**(s) as a trajectory with the variable *s* signifying position along the trajectory. As shown in Appendix B, the Hamilton-Jacobi partial differential equation (10) is equivalent to a set of ordinary differential equations for **x**(s) and **p**(s), the characteristic equations:

$$\frac{d\mathbf{x}}{ds} = 2\frac{\mathbf{D}}{\varphi_k} \cdot \mathbf{p} - \frac{\mathbf{q}}{\varphi_k} \tag{11}$$

$$\frac{d\mathbf{p}}{ds} = -\mathbf{p}^T \cdot \nabla\left(\frac{\mathbf{D}}{\varphi_k}\right) \cdot \mathbf{p} + \nabla\left(\frac{\mathbf{q}}{\varphi_k}\right) \cdot \mathbf{p}, \tag{12}$$

given here in vector-matrix form. Note that equation (11) is a generalization of the ray equation for the trajectory **x**(s), derived by *Smith* [1981] for a scalar dispersion coefficient. Integrating these equations results in expressions for the trajectory **x**(s) along which a solution is constructed. This is what is meant by a trajectory-based solution for transport. For the fully general case of anisotropic dispersion, the solution of equations (11) and (12) requires numerical integration. However, there are a number of efficient and well established algorithms to accomplish this [*Press et al*., 1992, p. 701].

The main task of this section is to determine the phase $\theta(\mathbf{x}, \omega)$, the solution of equation (8). Our approach is to formulate an additional ordinary differential equation for θ along with the trajectory defined by equations (11) and (12). That is, we consider θ as a function of **x**(s), using the chain rule

$$\frac{d\theta}{ds} = \nabla\theta \cdot \frac{d\mathbf{x}}{ds} = \mathbf{p} \cdot \frac{d\mathbf{x}}{ds}.$$

Substituting for the derivative of **x**(s) from equation (11) gives

$$\frac{d\theta}{ds} = 2\mathbf{p} \cdot \frac{\mathbf{D}}{\varphi_k} \cdot \mathbf{p} - \mathbf{p} \cdot \frac{\mathbf{q}}{\varphi_k},$$

which may be solved in conjunction with equations (11) and (12) via numerical integration.

Note that in streamline-based techniques, one adopts the trajectory defined by a simplification of the first set of ray equations (11)

$$\frac{d\mathbf{x}}{ds} = -\frac{\mathbf{q}}{\varphi_k} \tag{13}$$

as the path, rather than the exact ray path. There are several factors that make this a popular alternative. First, given the flow field **q**, say one obtained from a numerical simulation, the computation of the trajectory

x(s) is an elementary undertaking. Second, the trajectory obtained from equation (13) has a useful physical interpretation as a streamline of the flow field. The literature on streamline computation and streamline-based fluid flow modeling is extensive [e.g. *Datta-Gupta and King*, 2007]. Third, substituting equation (13) in place of the first set of equations (11) effectively decouples the system, allowing **x**(s) and **p**(s) to be computed independently. Only the spatial derivatives of $\mathbf{D}/\varphi_k$ and $\mathbf{q}/\varphi_k$ are required in the second set of equations (12), the coordinates of the trajectory do not appear explicitly. However, some of the physical connection between **x**(s) and **p**(s) will be lost if our trajectory deviates from the exact ray path. Fourth, as the dispersion diminishes, that is **D** approaches zero, the approximation (13) becomes increasingly accurate. In fact, the relative size of the terms on the right-hand-side of the first set of differential equations, equation (11), provides a measure of the accuracy of the approximation. Finally, we point out that the adoption of equation (13) is not entirely ad hoc. Rather, there is some freedom in the construction of an asymptotic solution, both in the specification of the power series expansion and in the partitioning of the solution into phase and amplitude components. Thus, by adopting an asymptotic approach based upon variables related to the square of scale parameter, $\mathbf{X}=\varepsilon^2\mathbf{x}$, advocated by *Gardner and Morikawa* [1960] for dispersive processes, *Vasco and Finsterle* [2004] arrived at an equation for the trajectory that is identical to equation (13). Compensation for the difference in the formulation appeared in the form of a diffusion equation for the amplitude, in the place of the transport equation that we introduce in the next subsection.

2.2.2. An Equation for the Amplitude

In order to construct the lowest (zeroth) order estimate for $C(\mathbf{x},\omega,\theta)$ in the series representation (6), we need both the phase $\theta(\mathbf{x},\omega)$ and the zeroth-order amplitude $C_0(\mathbf{x},\omega)$. In Appendix A, it is shown that the consideration of the terms of order ϵ in the asymptotic expansion produces an equation for the zeroth-order amplitude $C_0(\mathbf{x},\omega)$:

$$\boldsymbol{\Upsilon}\cdot\nabla \ln C_0=\upsilon, \tag{14}$$

where the coefficients $\boldsymbol{\Upsilon}$ and υ are defined in Appendix A in terms of **D**, **p**, **q,** and their derivatives (see equations (A14) and (A15)). Because equation (14) is a linear, first-order partial differential equation for the scalar quantity $C_0(\mathbf{x},\omega)$, it may be solved in a straight-forward fashion, either numerically along the trajectory, or in a semianalytic fashion [*Kravtsov and Orlov*, 1990]. Therefore, we shall assume that a solution of equation (14) is readily available in the discussion that follows.

2.3. An Expression for the Concentration

Armed with equations defining the trajectory **x**(s), the phase $\theta(\mathbf{x}(s),\omega)$, and the zeroth-order amplitude $C_0(\mathbf{x}(s),\omega)$, one can construct the zeroth-order expression for the concentration in the frequency domain

$$C(\mathbf{x},\omega)=e^{\theta(\mathbf{x},\omega)}C_0(\mathbf{x},\omega). \tag{15}$$

This expression is simply the first term in the power series expansion (6). A time domain expression for the concentration follows from an application of the inverse Fourier transform. To do this we make use of the fact that the inverse Fourier transform of a product in the frequency domain is a convolution of the terms in the time domain. Thus, the expression for the concentration in the time domain has the form

$$c(\mathbf{x},t)=\mathcal{F}^{-1}\left[e^{\theta(\mathbf{x},\omega)}\right]*c_0(\mathbf{x},t), \tag{16}$$

where $\mathcal{F}^{-1}$ denotes the inverse Fourier transform and * denotes a convolution. The function $c_0(\mathbf{x},t)$ is the inverse Fourier transform of the zeroth-order amplitude function. If the phase $\theta(\mathbf{x},\omega)$ is a general function of frequency, the quantity in brackets in equation (16) does not have a simple analytic inverse Fourier transform. That is not a barrier to the construction of a solution because one can easily perform the inverse Fourier transform numerically, using the fast Fourier transform [*Press et al*., 1992]. Therefore, expression (16) provides an efficient approach for calculating the temporal variation in the concentration at a point. For large values of ω, one can consider the high-frequency limit, leading to a semianalytic expression for the concentration variation as a function of time. Alternatively, if dispersion can be neglected, then the phase function simplifies and a semianalytic expression can also be found. These two cases are discussed in more detail in the subsections that follow. But first, we address the case of a general phase function, specified by equation (16).

2.3.1. A General Variation in Concentration

As shown in the Appendix C, one may reduce equation (10) to a quadratic equation for $p=|\mathbf{p}|$ (see equation (C16)):

$$\beta p^2 - \gamma p + i\omega\varphi_k = 0, \tag{17}$$

where

$$\beta = \sum_{i=1}^{3} D_i \cos\mu_i \cos\nu_i, \tag{18}$$

and

$$\gamma = q\cos\eta \tag{19}$$

with $q=|\mathbf{q}|$, and η is the angle between the vectors **p** and **q**. As indicated in Appendix C, μ_i is the angle between the vector **p** and a vector $\mathbf{u}_i$ from the singular value decomposition (SVD) of **D**. Similarly ν_i are the angles between **p** and $\mathbf{v}_i$, a member of the other set of vectors from the decomposition of the dispersion matrix. If the matrix is symmetric, then the sets of vectors are equivalent, that is $\mathbf{v}_i = \mathbf{u}_i$. Equation (17) is a quadratic equation that may be factored to produce an explicit, analytic expression for p. The fundamental parameters contained in these coefficients are D_i, q, and φ_k. Note that the magnitude of the Darcy velocity will depend upon the permeability and the pressure field or hydraulic head via Darcy's law (see equation (2)).

For a dispersive medium, β is nonzero and we must consider the full quadratic equation (17). The two solutions of the quadratic are readily found to be:

$$p = \frac{\gamma}{2\beta} \pm \frac{\sqrt{\gamma^2 - 4\beta\varphi_k i\omega}}{2\beta}. \tag{20}$$

By squaring the factored form (20) and using the fact that

$$p^2 = \nabla\theta \cdot \nabla\theta, \tag{21}$$

one arrives at an eikonal equation governing the propagation of transported material:

$$\nabla\theta \cdot \nabla\theta = \left[\frac{\gamma}{2\beta} \pm \frac{\sqrt{\gamma^2 - 4\beta\varphi_k i\omega}}{2\beta}\right]^2. \tag{22}$$

The eikonal equation is a fundamental equation, appearing in ray-based models of wave propagation [*Kline and Kay*, 1979; *Kravtsov and Orlov*, 1990; *Chapman*, 2004].

In the characteristic coordinate system, determined by the trajectories **x**(s), equation (20) may be integrated with respect to s, the distance along the trajectory, resulting in an expression for $\theta(\mathbf{x},\omega)$

$$\theta(\mathbf{x},\omega) = \int_{\mathbf{x}} \frac{\gamma}{2\beta} ds \pm \int_{\mathbf{x}} \frac{\sqrt{\gamma^2 - 4\beta\varphi_k i\omega}}{2\beta}\, ds. \tag{23}$$

It will be helpful in the discussion that follows to define the functions

$$\xi(\mathbf{x}) = \int_{\mathbf{x}} \frac{\gamma}{2\beta} ds \tag{24}$$

and

$$\chi(\mathbf{x},\omega) = \int_{\mathbf{x}} \frac{\sqrt{\gamma^2 - 4\beta\varphi_k i\omega}}{2\beta} ds, \tag{25}$$

so that we can write $\theta(\mathbf{x},\omega)$ more succinctly as

$$\theta(\mathbf{x},\omega) = \xi(\mathbf{x}) \pm \chi(\mathbf{x},\omega). \tag{26}$$

The time-domain solution is obtained by substituting this expression for $\theta(\mathbf{x},\omega)$ into equation (16) and performing the inverse Fourier transform followed by the convolution.

As an illustration, consider the case of tracer transport in a two-dimensional, uniform flow field. An analytic solution was published in *Javandel et al.* [1984], based upon the work of *Cleary and Ungs* [1978]. The solution corresponds

Table 1. Table Containing the Parameters for the Uniform and the Dipole Tracer Calculations

Category	Parameter	Description (Units)	Uniform Flow Field	Dipole Flow Field
Porous medium	φ_n	Porosity (fraction)	0.20	0.20
	k	Intrinsic permeability (m^2)	1.24×10^{-10}	1.24×10^{-10}
	α_l	Longitudinal dispersivity (m)	Variable	0.00
	α_t	Transverse dispersivity (m)	0.20	0.00
	d_m	Molecular diffusion (m^2/s)	0.00	Variable
Flow field	q	Darcy velocity (m/s)	2.00×10^{-4}	Variable

to a step-like injection along a linear segment of length $2a$, oriented perpendicular to a uniform flow field, where a is 5 cm in our example. The source is located on the y axis (flow along the x axis), and the solution is given by

$$c(x,y,t)=\frac{C_0 x}{4\sqrt{\pi D_l}}\exp\left[\frac{qx}{2D_l}\right]\int_0^{t/R}\exp\left[-\frac{q^2}{4D_l}\tau-\frac{x^2}{4D_l\tau}\right]\times\left[\mathrm{erf}\left(\frac{a-y}{2\sqrt{D_t\tau}}\right)+\mathrm{erf}\left(\frac{a+y}{2\sqrt{D_t\tau}}\right)\right]\tau^{-3/2}d\tau$$

where C_o is the injection rate of the solute. We have differentiated the response with respect to time in order to generate an impulse response. This differentiation relieves us of the task of evaluating the integral in this solution. In this example, we will consider an isotropic medium where the dispersion is characterized by transverse (D_t) and longitudinal (D_l) coefficients given by equations (3) and (4). In this example, we shall vary the longitudinal dispersivity while keeping the base parameters fixed (see Table 1). In Figure 1, we plot the temporal variation in concentration observed at a point 120 m directly downstream of the source for three values of α_l, the longitudinal dispersivity. For comparison, we also plot the asymptotic solution, given by the expression (16) where $\theta(\mathbf{x},\omega)$ is provided by equation (23). The two solutions are very similar for all times and for all three of the cases that we considered. In Figure 2 (top), we compare the analytic and asymptotic solutions to a numerical estimate computed using the T2DM dispersion model for TOUGH2 [*Oldenburg and Pruess*, 1993, 1996]. The numerical estimates appear to predict concentrations in the tail that are significantly larger than the analytic solution. This may reflect numerical dispersion, an effect that was noted in *Oldenburg and Pruess* [1993], particularly for coarser meshes. The effect may be exaggerated somewhat by the normalization of the curves.

2.3.2. A Rapid Variation in Concentration

For a general solution of the form (16), we can compute the concentration numerically. However, due to the complexity of the expression (23) for the phase, we cannot derive an analytic expression for the variation in the time domain. If we consider a concentration that is varying rapidly in time, relative to the background or natural variation, then a semianalytic expression is possible. In such a case, one can assume that the frequency of the variation, ω, approaches a large value. Therefore, we can consider the function $\chi(\mathbf{x},\omega)$, defined by the expression (25), in the limit of large frequencies. First, equation (25) is rearranged by factoring out $\sqrt{-i\omega}$ from the square root

$$\chi(\mathbf{x},\omega)=\sqrt{-i\omega}\int_{\mathbf{x}}\sqrt{1+\omega^{-1}\delta}\sqrt{\frac{\varphi_k}{\beta}}ds \tag{27}$$

where

$$\delta=\frac{i\gamma^2}{4\beta\varphi_k}. \tag{28}$$

Then the limit as ω takes on large values is

$$\begin{aligned}\lim_{\omega\to\infty}\chi(\mathbf{x},\omega)&=\lim_{\omega\to\infty}\sqrt{-i\omega}\int_{\mathbf{x}}\sqrt{1+\omega^{-1}\delta}\sqrt{\frac{\varphi_k}{\beta}}ds\\ &\approx\sqrt{-i\omega}\int_{\mathbf{x}}\sqrt{\frac{\varphi_k}{\beta}}ds.\end{aligned} \tag{29}$$

Thus, we can write the limit in a partitioned form

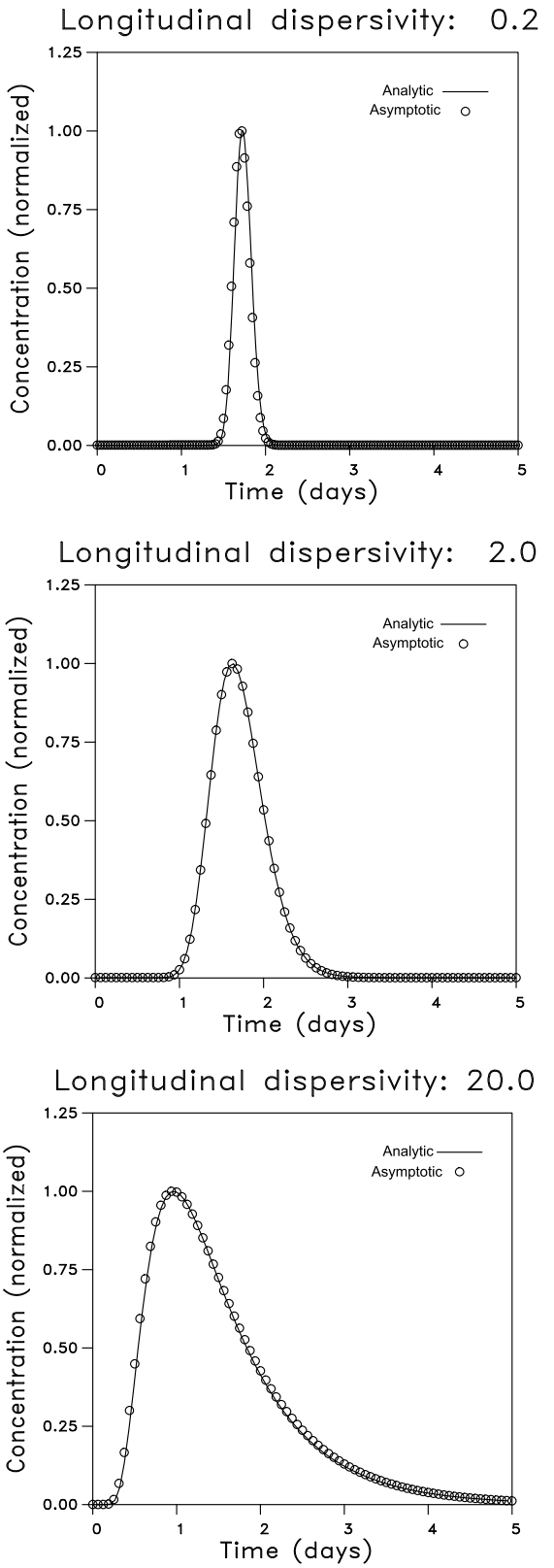

Figure 1. A comparison of the analytic solution of *Cleary and Ungs* [1978], as presented in *Javandel et al.* [1984] (solid lines) plotted with the asymptotic solution (open circles) obtained when the phase (23) is used in equation (16) to calculate the concentration. An impulsive or delta-function is used for the source-time function $c_o(\mathbf{x}, t)$. Comparisons are made at three different longitudinal dispersivities (a) 0.2 m, (b) 2.0 m, and (c) 20.0 m.

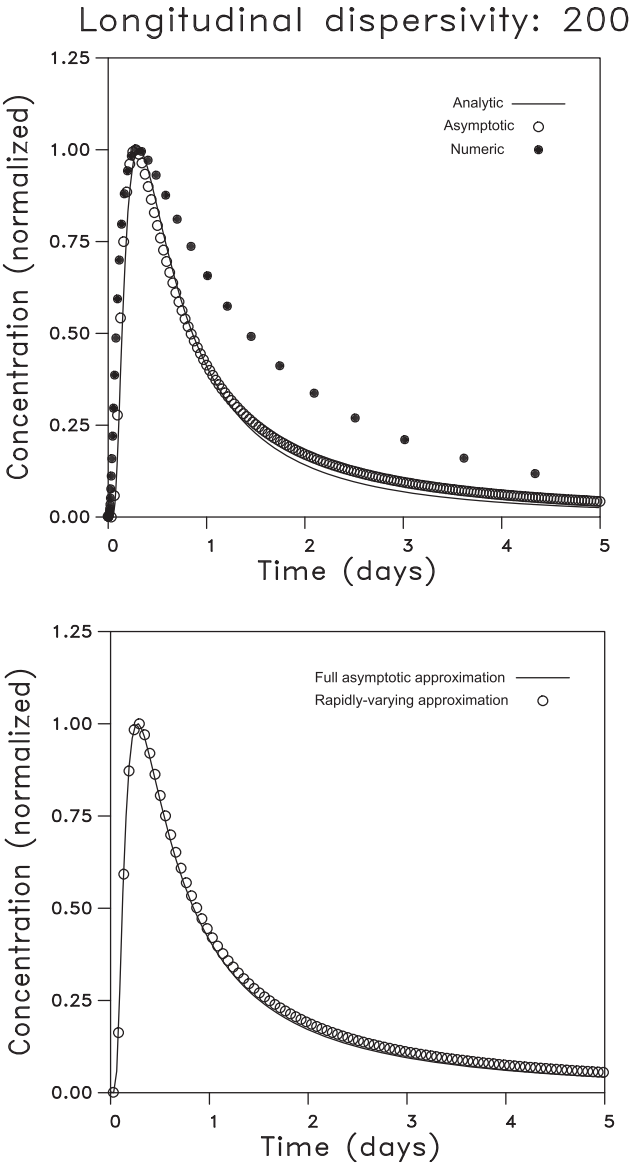

Figure 2. (top) Concentration estimates calculated using the analytic solution of *Cleary and Ungs* [1978] (solid line), the asymptotic solution (open circles), and the numerical solution of *Oldenburg and Pruess* [1993] (filled circles). (bottom) A comparison of the full asymptotic solution (solid line), which was also plotted in Figure 1, and the approximation (33) for a rapidly variation in tracer concentration.

$$\lim_{\omega\to\infty}\chi(\mathbf{x},\omega)=\sqrt{-i\omega}\chi(\mathbf{x}) \tag{30}$$

where we denote the spatially dependent component of $\lim_{\omega\to\infty}\chi(\mathbf{x},\omega)$ as

$$\chi(\mathbf{x})=\int_{\mathbf{x}}\sqrt{\frac{\varphi_k}{\beta}}ds. \tag{31}$$

The inverse Fourier transform of e^{θ}, the quantity in square brackets in equation (16), may now be evaluated analytically [*Virieux et al.*, 1994],

$$\mathcal{F}^{-1}\left[e^{-\sqrt{-i\omega}\chi(\mathbf{x})}\right]=\frac{\chi(\mathbf{x})}{2\sqrt{\pi t^3}}\exp\left[\frac{-\chi^2(\mathbf{x})}{4t}\right]H(t), \tag{32}$$

were we have taken the minus sign in equation (26), and $H(t)$ is the Heaviside (step) function that is 0 for negative values and 1 for nonnegative values. The complete expression for the time-varying concentration is given by

$$c(\mathbf{x},t)=\frac{\chi(\mathbf{x})}{2\sqrt{\pi t^3}}\exp\left[\xi(\mathbf{x})-\frac{\chi^2(\mathbf{x})}{4t}\right]H(t)*c_0(\mathbf{x},t) \tag{33}$$

for an impulsive source-time function. For a general time-varying source, we simply convolve expression (32) by the appropriate source-time function. In Figure 2 (bottom), we plot the approximation (33) against the full asymptotic solution, given by equations (16) and (23). The flow field and properties are identical to those used for the calculations associated with the results plotted in Figure 1 (see Table 1), while the dispersivity is larger (200 m). The approximation (33) generally agrees with the full asymptotic result even for this large value of longitudinal dispersivity.

2.3.3. A Nondispersive Porous Medium

Note that if the dispersion can be neglected then the matrix **D** may be taken to be zero in equation (8), or equivalently β vanishes in equation (17). Therefore equation (17) reduces to

$$p=i\omega\frac{\varphi_k}{\gamma}, \tag{34}$$

where γ is given by (19). If we orient our coordinate system so that the trajectory is tangent to **p** and use the definition of **p**, equation (9), to integrate (34) along the path and derive an expression for the phase

$$\theta(\mathbf{x},\omega)=i\omega\tau(\mathbf{x}) \tag{35}$$

where we have defined the function $\tau(\mathbf{x})$ as

$$\tau(\mathbf{x}) = \int_{\mathbf{x}} \frac{\varphi_k}{\gamma} ds. \tag{36}$$

The zeroth-order expression for the concentration may now be written as

$$C(\mathbf{x}, \omega) = e^{i\omega\tau(\mathbf{x})} C_0(\mathbf{x}, \omega). \tag{37}$$

Taking the inverse Fourier transform of (37) gives

$$c(\mathbf{x}, t) = c_0(\mathbf{x}, t - \tau(\mathbf{x})), \tag{38}$$

indicating that the concentration is a shifted version of the Fourier transform of the zeroth-order amplitude function. Note that there will generally be changes in the amplitude with propagation due to attenuation introduced by the transport, hence the dependence of the amplitude on the position along the trajectory **x**(s).

3. Applications

In this section, we illustrate the construction of trajectories associated with transport in a porous medium. That is, given the flow field from a numerical simulation, we calculate the paths **x**(s) along which our semianalytic solutions are defined. The advantage of the semianalytic expressions are that they provide a clear relationship between the flow parameters and characteristics of the tracer breakthrough curve, and yet are valid in a medium with smoothly varying properties. We conclude this section with an application to a laboratory experiment in which injected brine is monitored using X-ray computed tomography (CT). Here we introduce the onset time of a change in the X-ray attenuation and demonstrate how these times may be used to estimate the hydraulic conductivity variation in a laboratory sample. That is, the semianalytic expressions are the basis for a fast tomographic inversion for hydraulic conductivity.

3.1. Numerical Illustrations

While the mathematical derivation of the asymptotic solution, given in Appendix A, is fairly involved, the construction of the zeroth-order solution is relatively straight-forward. It is instructive to examine in detail how one determines the trajectories, using the output from a numerical simulator. Here, we use the integral finite-difference simulator TOUGH2 [*Oldenburg and Pruess*, 1995, 1996; *Pruess et al*., 1999] for our calculations. The numerical simulation provides critical information for the asymptotic solution, in particular the flow field **q** that appears in the characteristic differential equations (11) and (12) defining the trajectory **x**(s). The procedure is similar to that used in streamline simulation [*Crane and Blunt*, 1999; *Datta-Gupta and King*, 2007] in that a numerical technique, such as finite differences, is used to compute the pressure field defining the streamlines. However, unlike a streamline, the path of a trajectory, **x**(s) depends upon the full matrix **D**. Therefore, as is evident in equations (11) and (12), the trajectory depends upon **q**, **D**, and φ_k. In order to maintain continuity with past analytical and numerical results, we adopt the symmetric form of the dispersion tensor for an isotropic medium

$$\mathbf{D} = D_t \mathbf{I} + (D_l - D_t)\hat{\mathbf{q}}\hat{\mathbf{q}} \tag{39}$$

[*Oldenburg and Pruess*, 1995, 1996] to represent the dispersion tensor **D** for the comparisons in this subsection. The vector $\hat{\mathbf{q}}$ is a unit (normalized) vector in the direction of **q** and the principle values D_l and D_t are given by equations (3) and (4), respectively. As noted above, our development is not limited to this case, the formulation is in terms of a general anisotropic tensor **D**.

3.1.1. A Uniform Flow Field

We first consider tracer transport in a uniform flow field. In this simulation, the nodes at the left (western) edge of the model each inject 3 kg/s of fluid while the rightmost nodes produce fluid at the same rate. There are no-flow boundary conditions at the northern and southern edges of the model and constant pressure boundaries at the east and west boundaries. The resulting pressure field, computed using the numerical simulator TOUGH2, is plotted in Figure 3 along with the location of the tracer injector (filled square) and the observation point (open circle). The tracer injection rate of 0.001 kg/s is so small that it has minimal influence on the fluid pressure distribution, and similarly for

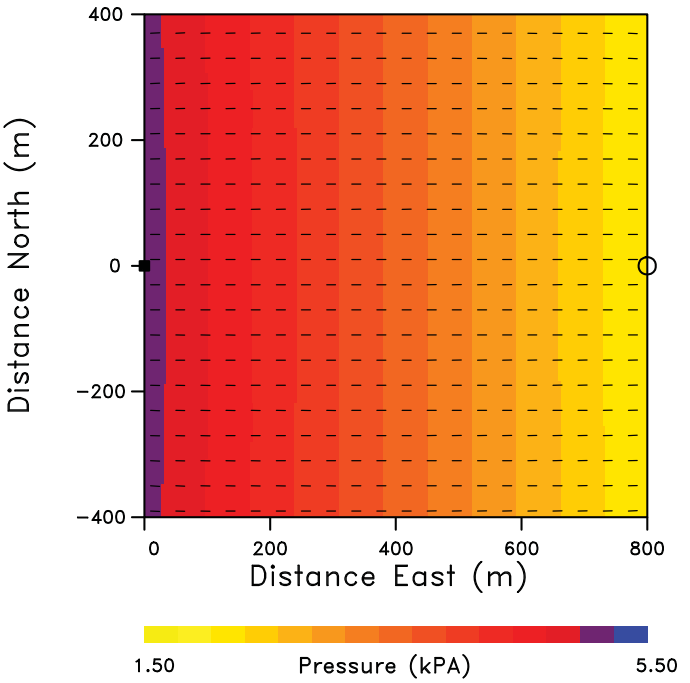

Figure 3. A pressure field that is nearly uniform along the *y* axis. The tracer injection point is denoted by the filled square while the observation point is located at the open circle. The color variations indicate the pressure field values. The short line segments indicate the direction of the flow vector **q**.

the observation well. The unit vector field in the direction of the pressure gradient, $\hat{\mathbf{q}}$, is also plotted in Figure 3.

The distribution of tracer was computed using the analytical solution of *Cleary and Ungs* [1978] given in *Javandel et al*. [1984], as it does not suffer from the numerical dispersion characteristic of reservoir simulators. The solution was differentiated with respect to time in order to produce the response to an impulsive tracer source function. Three cases are considered. In each case, the porosity of the medium is 0.2 and the longitudinal dispersivity is 20.0 m, while the transverse dispersivity takes the values 20.0, 2.0, and 0.2 m, respectively. The resulting concentration distributions after 7 days are plotted in Figure 4. The effect of decreasing transverse dispersion is clear by the narrowing of the tracer distribution.

The contributions to the trajectory **x**(s) are evident by the terms on the right-hand side of equation (11). The pressure field supplied by TOUGH2 is used to calculate the fluid velocity and hence **q**. The expression for **D**, given above, indicates how **q** contributes to the elements of the dispersion matrix. In particular, we can substitute equation (39) for **D** into the expression for the tangent vector for the paths, equation (11), resulting in

$$\frac{d\mathbf{x}}{ds} = \frac{2}{\varphi_k} D_t \mathbf{p} + \frac{1}{\varphi_k}\left[2(D_l - D_t)\mathbf{p}\cdot\hat{\mathbf{q}} - \frac{q}{\varphi_k}\right]\hat{\mathbf{q}}. \tag{40}$$

Because the flow field is uniform in space and does not change as we vary D_l and D_t, the primary deviations are due to changes in the phase gradient vector $\mathbf{p}=\nabla\theta$. In Figure 5, contours of the phase $\theta(\mathbf{x})$ are plotted

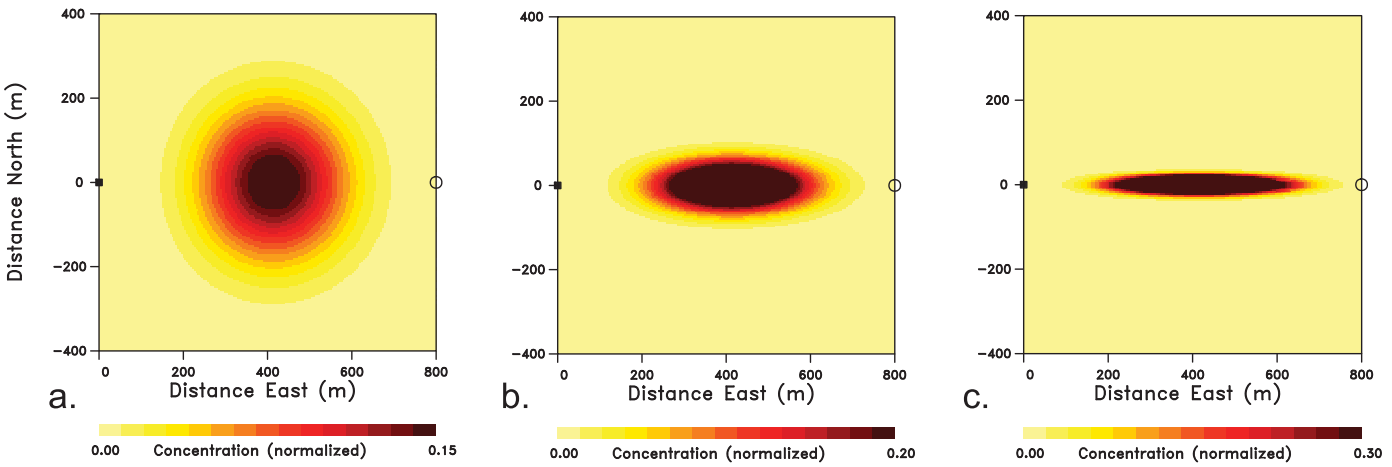

Figure 4. Snapshots of the tracer concentration distribution after 7 days of uniform flow. In all three cases, the longitudinal dispersivity (α_l) is 20 m while the transverse dispersivity (α_t) is 20.0 m (a), 2.0 m (b), and 0.2 m (c), respectively.

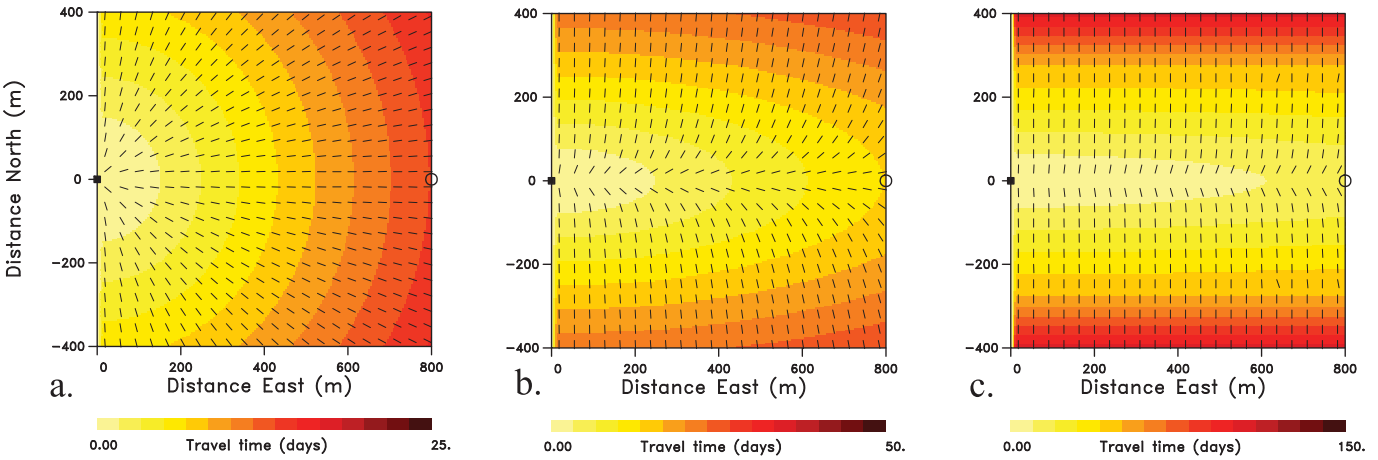

Figure 5. The tracer travel times for the three cases considered in Figure 4. The line segments denote the directions of the normalized phase gradient vector field.

along with the unit vector fields $\hat{\mathbf{p}}$ that are normal to the contours. These contributions cause the trajectories to deviate from streamlines that follow **q**.

A Runge-Kutta routine with adaptive step size control is used to solve the system of equations (11) and (12) [*Press et al*., 1992, p. 714]. The resulting trajectories are plotted in Figure 6, along with the magnitude of the tracer concentration, normalized by the concentration 100 m downstream of the source. The angular distribution of the trajectories extends from -80.0 to $+80.0$ degrees with respect to the line connecting the source and the observation point. Most of the trajectories plotted in Figure 6 bend sharply at the source and then straighten. The areas containing the highest density of trajectories coincide with the largest tracer concentrations, calculated using the analytic solution.

3.1.2. A Dipole Tracer Test

Next, we consider the situation in which there are two wells in communication, as illustrated in Figure 7. A flow field is first set up by injecting fluid into one well while an equal amount of fluid is extracted from an adjacent well. After the transient effects have decayed and a steady state pressure field has been obtained, a chemical tracer is introduced into the injection well. The resulting tracer distribution, computed using the T2DM variant of TOUGH2 [*Oldenburg and Pruess*, 1995, 1996], is plotted in Figure 7 for three different times (5, 15, and 50 days). In Figure 8, we indicate the flow vector field **q** (left) and the phase gradient vector field $\mathbf{p}=\nabla\theta$ orthogonal to the phase contours (right). The vector fields have been normalized to unit amplitudes.

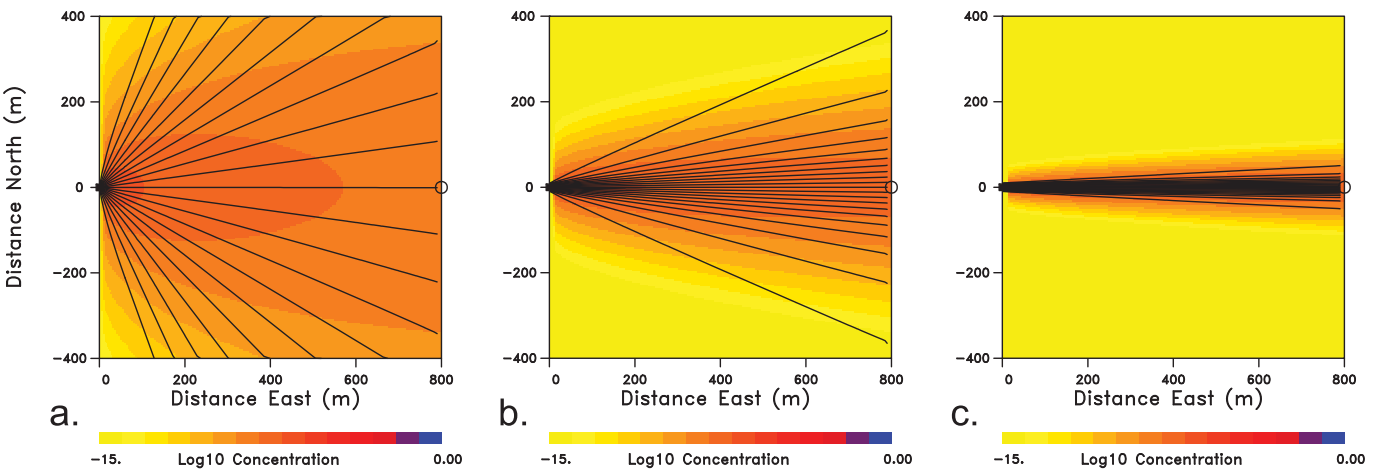

Figure 6. Twenty-one trajectories, plotted as black lines, corresponding to the movement of the tracer, obtained by solving the differential equations (11) and (12). The background color variation denotes the spatial variation of peak tracer magnitude for each grid block. The concentration magnitudes have been normalized by the value 100 m downstream from the injection point.

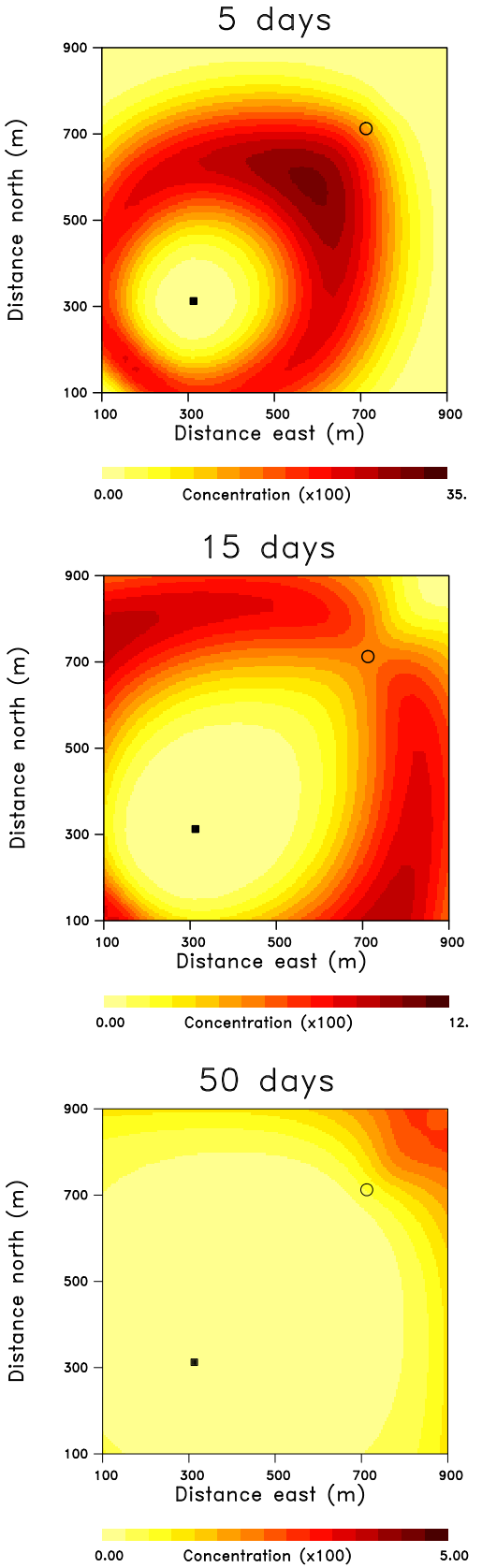

Figure 7. Tracer concentration snapshots for three different times (5, 15, and 50 days after the start of injection) for a dipole tracer test. The longitudinal and transverse dispersivities are both 20. The molecular diffusion is set equal to 0 in this case.

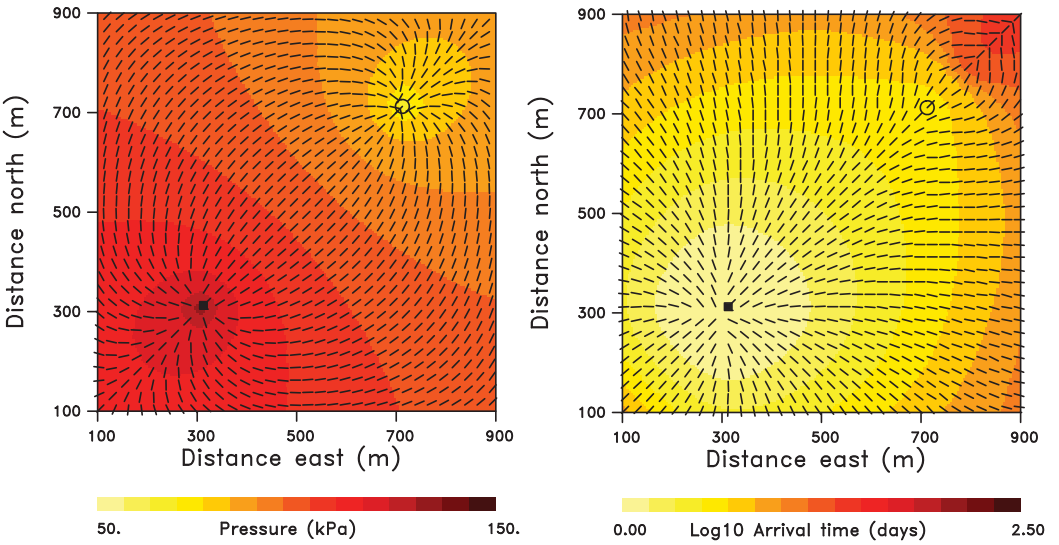

Figure 8. (left) Pressure field associated with the dipole test. The line segments denote the normalized flow vector $\hat{\mathbf{q}}$ directions. (right) Arrival times of the peak tracer at various points on the simulation grid. The line segments denote the direction of the normalized phase gradient vector, $\mathbf{p}=\nabla\theta$.

As indicated above, the two vector fields influence the trajectories representing the movement of the tracer. The resultant vector field, the right-hand-side of equation (40), associated with the case $\alpha_l=\alpha_t=20$ *m*, is plotted in Figure 9 (left). The trajectories $\mathbf{x}(s)$, computed using the Runge-Kutta method to solve equations (11) and (12), are locally tangent to the unit vectors (Figure 9). In Figure 9 (right), we plot the corresponding streamlines associated with the flow field. In this case, the trajectories deviate significantly from conventional streamlines.

In Figure 10, we explore the influence of variations in molecular diffusion, d_m in equations (3) and (4), on the trajectories. In particular, we consider four cases in which the dispersivities α_l and α_t are zero while the molecular diffusion coefficient takes on small but finite values. For the first case, corresponding to Figure 10a, the molecular diffusion coefficient is set at 2.0×10^{-9}. Here, most trajectories extend from the injection well to the production well, while a few propagate outward to the edge of the simulation grid. The trajectories are essentially identical to the streamlines plotted in Figure 9. For larger values of *d*, the

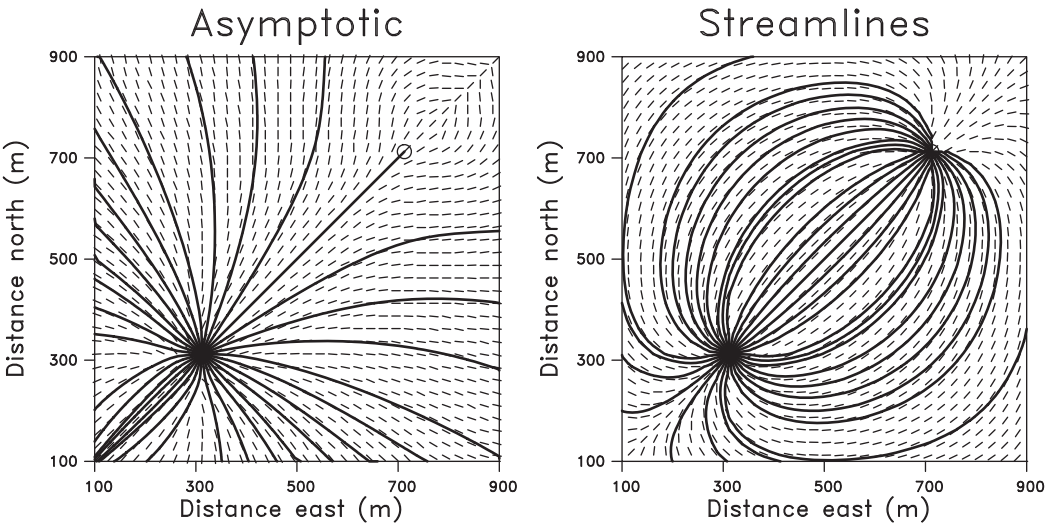

Figure 9. (left) Trajectories calculated using equations (11) and (12). The line segments denote the normalized tangent vector field, constituting the right-hand-side of equation (40). (right) Streamlines obtained by solving equation (13). The line segments denote the direction of the normalized flow field $\hat{\mathbf{q}}$.

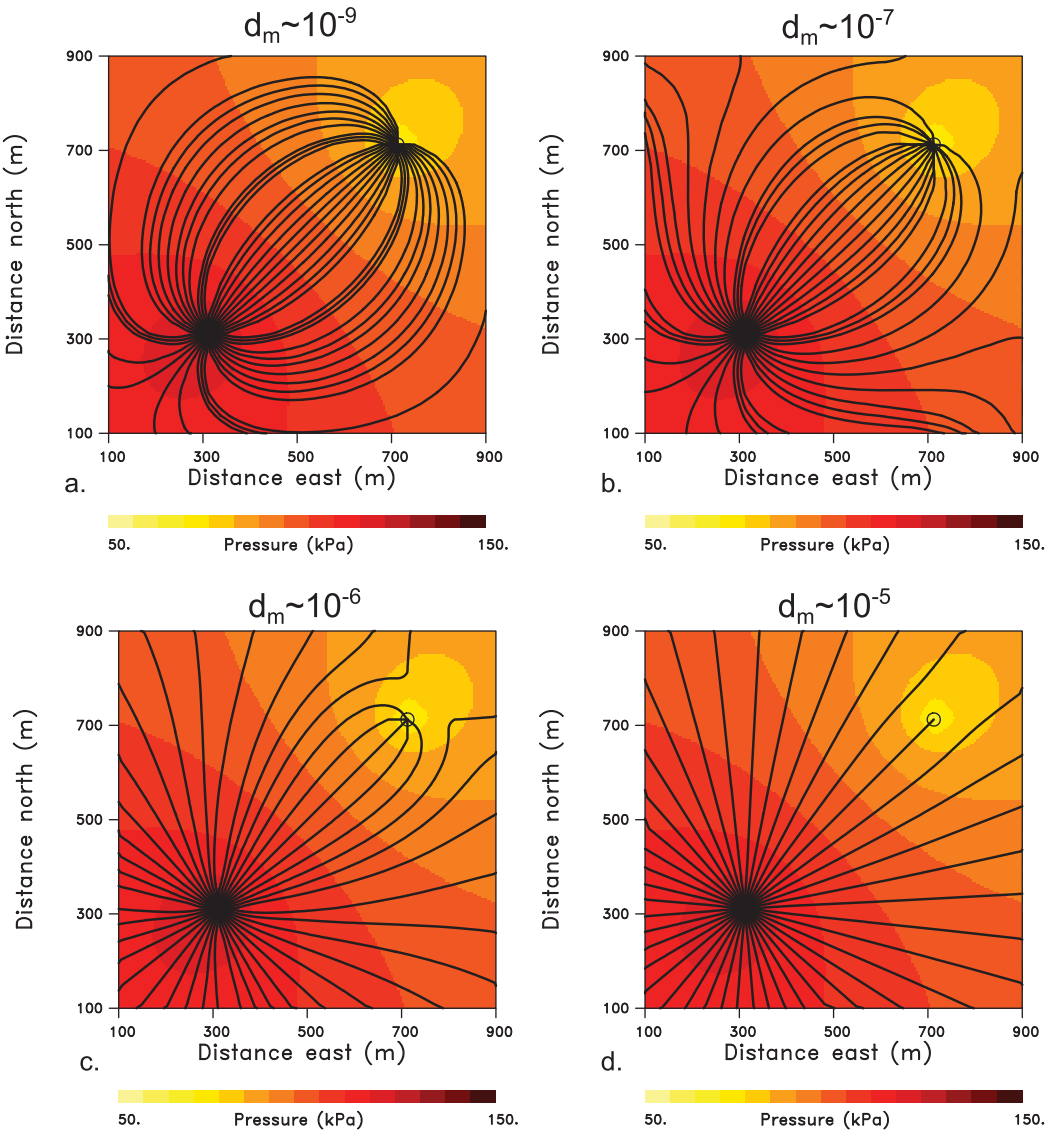

Figure 10. Trajectories associated with a dipole tracer configuration. The four sets of trajectories correspond to different values of molecular diffusion: (a) $d_m = 2.3\times10^{-9}$. (b) $d_m = 2.3\times10^{-7}$. (c) $d_m = 2.3\times10^{-6}$. (d) $d_m = 2.3\times10^{-5}$. For all of these cases, both the longitudinal and transverse dispersivities were zero.

trajectories diverge toward the outer boundary of the model, indicating that diffusion plays a significant role in the movement of the tracer in comparison to the flow field **q**. Because most common ions in fluids have molecular diffusion coefficients in the range 1×10^{-9} to 2×10^{-9} m^2/s [*de Marsily*, 1986, p. 233], diffusion will not induce much deviation from streamline geometry. However, diffusion in supercritical fluids can be an order of magnitude greater, and diffusion coefficients for ions in fluids such as supercritical carbon dioxide are greater than 10^{-8} m^2/s [*Sassiat et al*., 1987]. Furthermore, diffusion in gases can be much more significant, leading to molecular diffusion coefficients of the order of 10^{-5} m^2/s.

3.2. Application to the X-Ray Imaging of a Brine Injection Experiment

One important application of trajectory-based modeling is in solving the inverse problem, in which remote observations are used to infer flow properties, such as hydraulic conductivity or diffusivity, in a porous medium. Here we shall discuss an example of an inverse problem that is based upon the X-ray imaging of a laboratory fluid injection experiment. Brine was injected into a core of Bartlesville sandstone. The outer boundary of the core was a no-flow boundary while the inlet and outlet edges were at constant pressure. The long end of the core is parallel to the bedding within the sandstone. The cylindrical core was subjected

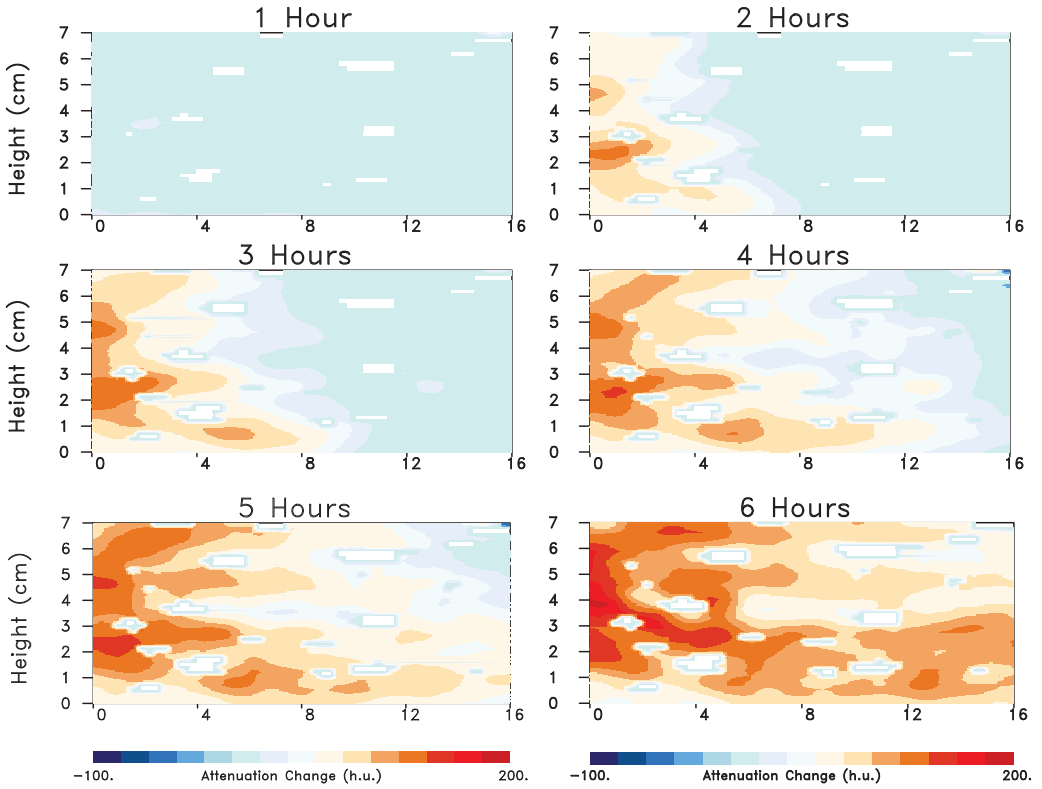

Figure 11. Six snapshots of X-ray attenuation due to the injection of a saline tracer into a core of Bartlesville sandstone. The color scale in each plot signifies the attenuation over a slice through the center of the sandstone core.

to repeated X-ray scanning to image the attenuation due to the increased salinity of the fluid within the sample. The sample was initially scanned every hour for the first 11 h, and after that at 24, 52, 70, and 100 h. The results of the first 6 h of imaging are shown in Figure 11 for a vertical slice through the middle of the three-dimensional image. Note the regions in the sample where the amplitudes saturate and are unreliable. These regions are indicated by the white pixels in Figure 11.

3.2.1. The Onset Time of X-Ray Amplitude Changes

While it is possible to use the changes in attenuation to estimate the changes in the salinity in a given volume element (voxel), there is a potential difficulty with that approach. The X-ray amplitudes are only indirectly related to changes in brine concentration and one must infer the concentration based upon a physical model. Thus, one would need to know coupling parameters and properties that may effect the attenuation, such as the average porosity within the voxel. Properties such as porosity may vary spatially, confounding a simple interpretation of the attenuation data. Given the hourly sampling, we can take an alternative approach to estimate effective hydraulic conductivity variations within the core. Rather than use the magnitude of the change in X-ray attenuation to infer the concentration change, we can use the time at which we begin to see a change in the attenuation within a voxel as a measure of the arrival time of the saline fluid within that voxel. We refer to this time as the onset time of the amplitude changes. It has been shown that, as long as the observations themselves are sensitive to changes in saturation and pressure, such onset times are much more sensitive to the flow properties than they are to the details of the rock physics model [*Vasco et al.*, 2014].

One can use the onset of increased attenuation, for each imaged voxel of the sample, to infer the arrival of the saline fluid throughout the core. There are several ways to define the onset of an attenuation change. For example, one can consider a threshold, say 5% of the peak change, and define the onset as the time as which the threshold is exceeded. Alternatively, one may associate the onset time of a change with the peak slope (derivative) of the curve. In what follows we shall use the threshold criterion to determine the onset as this works better with moderately noisy data. The onset of a change in amplitude is related to the arrival

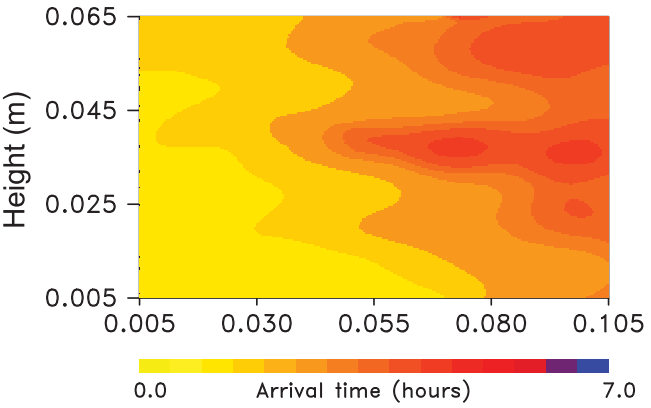

Figure 12. Onset time of the changes in X-ray attenuation from the background value.

of saline fluid within the sample. In Figure 12, we plot the arrival or onset times for a portion of the sample. We see that the fluid does not propagate uniformly through the sample, in agreement with the images in Figure 11. Rather, the fluid appears to move at different speeds, depending upon the height. Most likely this reflects the bedding within the sample and associated variations in hydraulic conductivity.

3.2.2. Relationship Between the Onset Time and Flow Properties

By causality, the onset time of attenuation change is assumed to correspond to the arrival time of the saline tracer. Because the onset of the change in attenuation is rather abrupt, we adopt the expression (33), for a rapid variation in concentration. In order to produce an expression for the arrival time, we follow a procedure advocated by *Virieux et al*. [1994] in which we consider the time at which a peak value is obtained. Because the source is step-like in nature, rather than impulsive, we consider the time derivative of the concentration, denoted by $\dot{c}(\mathbf{x},t)$. Then, the expression (33) will involve a convolution between the inverse transform (32) and a delta function (the time derivative of a step-function). Thus, away from the origin, the peak of the derivative is given by the vanishing of

$$\frac{\partial \dot{c}}{\partial t}=\frac{\chi}{2\sqrt{\pi t^3}}\exp(\xi)\exp\left(-\frac{\chi^2}{4t}\right)\left[\frac{\chi^2}{4\sqrt{t^7}}-\frac{3}{2\sqrt{t^5}}\right] \tag{41}$$

where we have suppressed the $\mathbf{x}$ dependence of $\xi(\mathbf{x})$ and $\chi(\mathbf{x})$. Away from the origin and ∞, the time derivative is a maximum when the quantity in the square brackets vanishes. Thus, the peak slope is attained at time T_{max}, given by

$$\sqrt{T_{\max}}(\mathbf{x})=\frac{1}{\sqrt{6}}\chi(\mathbf{x})=\frac{1}{\sqrt{6}}\int_{\mathbf{x}}\sqrt{\frac{\phi_k}{\beta}}ds \tag{42}$$

where we have used the definition (31) of $\chi(\mathbf{x})$ to relate the square root of T_{max} to the properties φ_k and β. This general approach has also been used for the inversion of transient pressure data [*Vasco et al*., 2000]. We can use definition (18) of β and the definitions (3) and (4) of the longitudinal and transverse dispersion to rewrite the integral in equation (42). As noted above, the molecular diffusion coefficient is typically rather small and does not influence the tracer propagation. Therefore, we will neglect the effect of molecular diffusion with respect to intrinsic dispersion. Furthermore, for this application we are assuming that the dispersion tensor $\mathbf{D}$ is symmetric and thus the angles μ_i and ν_i are equal in equation (18). Therefore, β takes the form

$$\beta=q\sum_{i=1}^{3}\alpha_i\cos^2\mu_i. \tag{43}$$

Making use of equation (2) for $\mathbf{q}$, and assuming that the hydraulic conductivity is isotropic, we can write (43) as

$$\beta=K|\nabla h|\sigma, \tag{44}$$

where σ represents the sum

$$\sigma=\sum_{i=1}^{3}\alpha_i\cos^2\mu_i. \tag{45}$$

Combining the expression (44) for β with equation (42) provides a semianalytic expression relating the square root of the onset time to the hydrologic properties of the medium

$$\sqrt{T_{\max}}(\mathbf{x}) = \frac{1}{\sqrt{6}}\chi(\mathbf{x}) = \frac{1}{\sqrt{6}}\int_{\mathbf{x}}\sqrt{\frac{\phi_k}{K|\nabla h|\sigma}}ds. \tag{46}$$

This semianalytic expression indicates the factors that influence the tracer arrival time. In particular, we note that the dispersivities impact the arrival time through the presence of σ in equation (46). It is evident in Figures 1 and 2, that the longitudinal dispersivity does indeed alter the arrival time, reducing it as α_l increases in value.

If we can neglect dispersion altogether, then the time-shift given by equation (36) can be used to calculate the onset time. Such a nondispersive solution was given in *Vasco and Datta-Gupta* [1999] and *Datta-Gupta et al.* [2002]. In that case, in the place of the square-roots there would be a direct relationship between the onset time and the flow properties. Also, the quantity σ would no longer be present in the integral expression.

If the spatial variation in dispersion, contained in σ, is much less than the spatial variation in hydraulic diffusivity (φ_k/K), then equation (46) provides a means to estimate the hydraulic diffusivity or the effective hydraulic conductivity $K(\mathbf{x})$ from the onset time data shown in Figure 12. Even though equation (46) provides a direct relationship between the onset time and the ratio φ_k/K, it depends upon the head or pressure field due to the presence of $|\nabla h|$ in the integrand and on the sum over the dispersivities σ. As indicated by equation (11), the trajectory itself, $\mathbf{x}(s)$, also depends upon the head or pressure field. Thus, we must solve equation (46), or a discretized version of it, in an iterative fashion, assuming some initial model and then successively updating the model and recalculating the pressure field in order to improve the fit to the observations.

3.2.3. Tomographic Imaging of Flow Properties

Assuming that the heterogeneity is dominated by the variations in hydraulic diffusivity, equation (46) allows us to devise a tomographic imaging algorithm for the hydraulic diffusivity or the effective hydraulic conductivity. In essence, we can use the arrival or onset times in Figure 12 as data, and the equation provides a semianalytic relationship between the onset times and the flow properties in the sample. The key point is that we only need to calculate the pressure field in order to set up the integral (42) because that allows us to evaluate the integrand given initial values for the porosity. From the pressure calculation, one can compute ∇h and we can use equations (11) and (12) to find the flow path given an initial estimate of the hydraulic conductivity. We can discretize the integral (46) into a sum for each trajectory, for the j-th trajectory we have

$$\sqrt{T_j} = \sum_{n=1}^{N}\sqrt{\frac{\varphi_n}{K_n}}\frac{l_{jn}}{\sqrt{\sigma_n|\nabla h_n|}}, \tag{47}$$

where l_{jn} is the length of the j-th trajectory in the n-th grid block. For a given pressure field, equation (47) is a linear equation for the square root of the diffusivity

$$\mathcal{D} = \sqrt{\frac{\varphi_n}{K}} \tag{48}$$

in each grid block. If the diffusivities, and hence σ, can be estimated, and do not vary significantly over the core, then equation (47) can be used to determine $\mathcal{D}$ is each grid block.

Because the pressure field depends upon K and φ_n, one must solve the equation iteratively, updating the pressure field and the trajectories at each step. We can use equation (47) to derive a relationship between a perturbation in $\mathcal{D}$ and a perturbation in the square root of the travel time,

$$\delta\sqrt{T_j} = \sum_{n=1}^{N}\frac{l_{jn}}{\sqrt{\sigma_n|\nabla h_n|}}\delta\mathcal{D}_n, \tag{49}$$

where the perturbation is signified by δ. Equation (49) can serve as the basis for an iterative updating scheme for estimating spatial variations in $\mathcal{D}$. That is, our collection of onset time deviations, denoted by $\delta\mathbf{d}$, provide constraints of the form (49), producing a system of linear equations for perturbations of the diffusivity in each voxel, $\delta\mathbf{y}$,

$$\delta\mathbf{d} = \mathbf{M}\delta\mathbf{y}, \tag{50}$$

where $\mathbf{M}$ is the coefficient matrix, with elements $M_{jn} = l_{jn}/\sqrt{\sigma_n|\nabla h_n|}$. We solve the system of equations (50) for the vector of perturbations, $\delta\mathbf{y}$, using an iterative solver. Because of variations in the flow geometry,

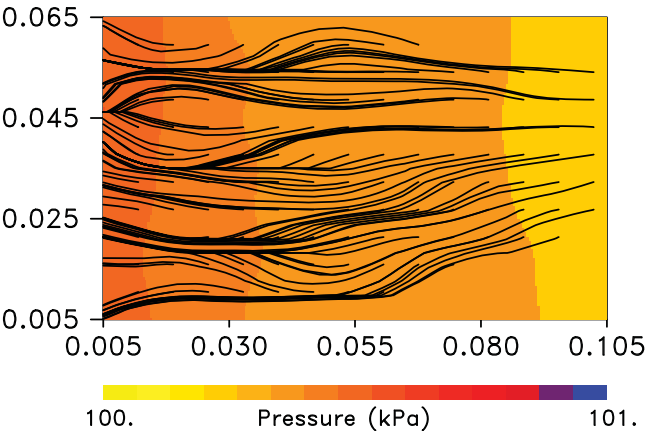

Figure 13. Selected trajectories associated with the final iteration of the inversion algorithm. In order to clearly see the trajectories, every third path is plotted in this figure. The background colors represent the variation in fluid pressure across the sample.

there may be grid blocks that are not traversed by any trajectories. Such grid blocks are poorly constrained and their presence will lead to difficulties in the numerical solution of the system of equations (50) for $\delta\mathbf{y}$. In order to stabilize the system, we can introduce an additional penalty term that biases the perturbations toward zero. The normal equations for the solution of the least squares problem take the form

$$\mathbf{M}^t\delta\mathbf{d}=(\mathbf{M}^t\mathbf{M}+W_n\mathbf{I})\delta\mathbf{y}, \qquad (51)$$

where $\mathbf{I}$ is the identity matrix and W_n is the weight or bias associated with minimizing the size of the perturbations from the existing model. We take a weighting parameter of $W_n = 1$. We solve this system of equations using an algorithm designed for solving sparse linear least squares problems [*Paige and Saunders*, 1982]. After 50 iterations of the linearized inversion algorithm, the squared misfit was reduced by 70% from its initial value. Our starting model has uniform properties with a porosity (φ_n) of 0.2, and a hydraulic conductivity of 3.2×10^{-6} m/s (intrinsic permeability of 3.24×10^{-13} m^2). Selected trajectories for the final iteration of the X-ray imaging problem are plotted in Figure 13. A total of 1680 trajectories were used in the inversion extending from each voxel to the inlet port. Trajectories near the upper and lower edges of the core were excluded from the inversion in order to avoid the effects of the boundaries on the flow. Each trajectory and associated onset time provides a linear constraint on the perturbations of hydraulic conductivity within the sample.

Note that, unlike conventional tomography, where one is only sampling over a single time interval, we are sampling over 11 successive time intervals. Thus, even though we do not have the crossing trajectories that are so essential in conventional tomography, due to the temporal sampling we have many trajectories that traverse portions of the same paths, but for different distances. And so the temporal sampling allows us to resolve changes along the path, and thus localize variations in $\mathcal{D}$ along the path. In many areas, trajectories appear to converge into the zones where the concentration propagates most rapidly. The corresponding hydraulic conductivity distribution is plotted in Figure 14. The heterogeneity appears to reflect the layering of the core with permeability variations that are dominantly horizontal. Areas of high conductivity correspond to regions where the tracer propagates the fastest.

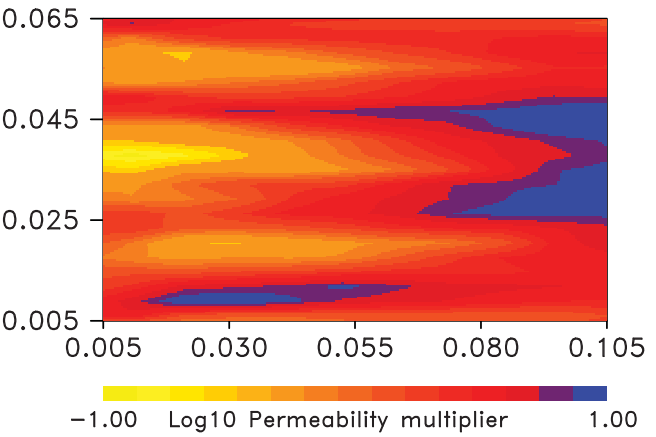

Figure 14. Deviations of the logarithmic multiplier from the uniform background starting value of 3.24×10^{-13} m^2.

We can use the model in Figure 14 to calculate the expected travel times to the observation points in the model. In Figure 15, we compare the observed and calculated travel times. In general, there is fair agreement between the observations and predictions based upon the hydraulic conductivity estimates, though there is significant scatter. The scatter may be due to the rather coarse temporal sampling of 1 h, which was necessary in the older X-ray imaging system used to gather the attenuation data. Such large time intervals between images limit the accuracy of our onset time estimates introducing significant uncertainties, of the order of 30 min.

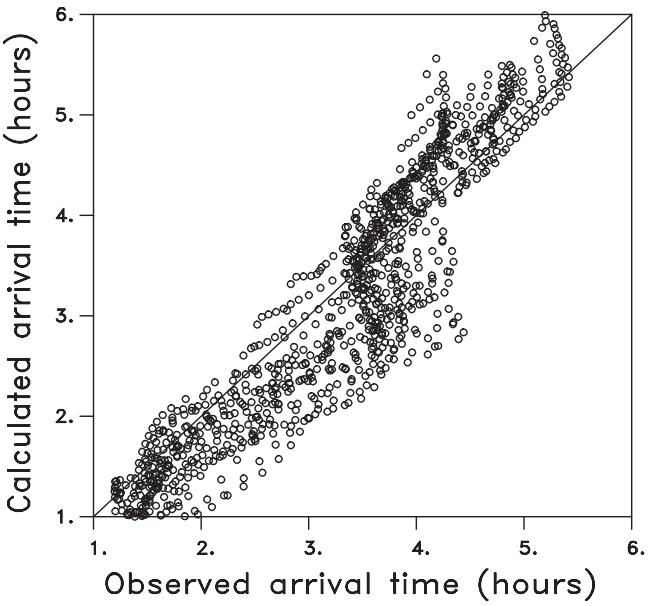

Figure 15. Calculated onset time plotted against the observed onset times for the 1680 values obtained by sampling the voxels in the X-ray imaging of the saline injection.

3.2.4. Model Assessment

While the imaging of flow properties is often the primary goal, model assessment is an equally important aspect of an investigation. An assessment entails calculating, at the very least, uncertainties associated with the estimated model parameters. In problems involving estimates of spatially varying quantities a model assessment typically includes some measure of spatial resolution [*Parker*, 1994; *Vasco et al*., 1997]. For linear inverse problems, there is a well-developed formalism for model assessments involving the computation of the model parameter resolution and covariance matrices [*Parker*, 1994]. Our model assessment is applied to the final iteration of our linearized inversion scheme, a common practice for nonlinear inverse problems.

Because the model parameter resolution matrix may be less familiar to readers, we briefly review its calculation. The resolution matrix follows from the constraint equations (50) and an expression for the solution of the inverse problem. For example, we could solve the regularized system of equations (51) for an estimate of $\delta\mathbf{y}$, producing

$$\delta\hat{\mathbf{y}} = \mathbf{M}^{\dagger}\,\delta\mathbf{d}, \tag{52}$$

where $\mathbf{M}^{\dagger} = (\mathbf{M}^t\mathbf{M} + W_n\mathbf{I})^{-1}\mathbf{M}^t$, and $\delta\hat{\mathbf{y}}$ denotes our estimate. Substituting for $\delta\mathbf{d}$ using equation (50) results in

$$\delta\hat{\mathbf{y}} = \mathbf{R}\delta\mathbf{y}, \tag{53}$$

where

$$\mathbf{R} = \mathbf{M}^{\dagger}\mathbf{M} \tag{54}$$

is the resolution matrix. Equation (53) highlights the fact that the resolution matrix **R** indicates how a hypothetical true solution is averaged to form an estimate. Thus, the rows of the resolution matrix are spatial averaging coefficients, indicating how various parts of the model contribute to a particular parameter estimate. The diagonal elements of the resolution matrix provide measures of the ability of the inversion algorithm to isolate particular model parameters. If we could solve the inverse problem with no averaging, then **R** would be the identity matrix. Thus, for well-resolved parameters the diagonal elements of **R** would be close to 1 while for poorly resolved parameters the diagonal elements would approach zero. In Figure 16, we plot the diagonal elements of the resolution matrix in the location of

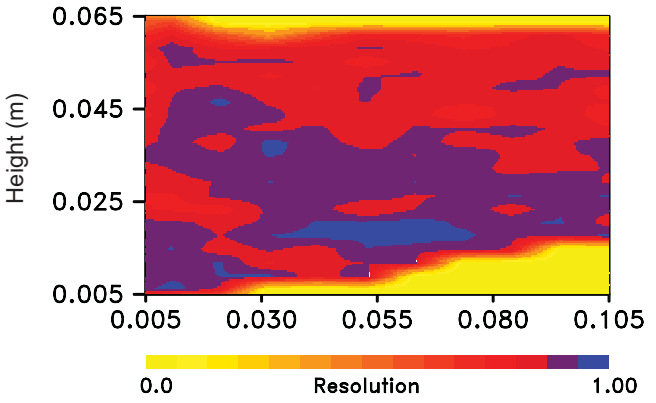

Figure 16. Diagonal elements of the model parameter resolution matrix, plotted in their associated grid block locations.

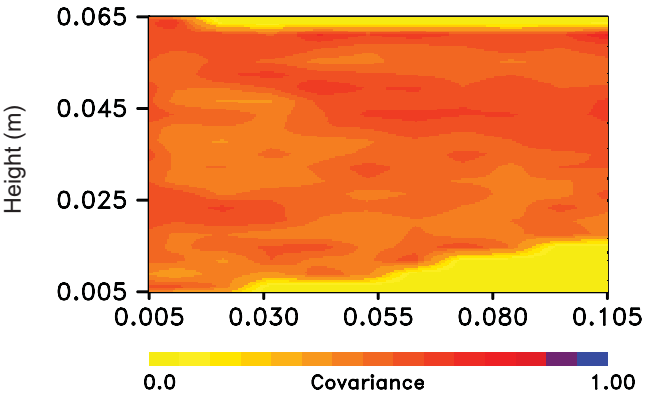

Figure 17. Model parameter standard errors associated with the estimates of the logarithmic multipliers that are plotted in Figure 14.

their corresponding grid block. From a comparison of Figures 13 and 16, we see that the resolution is quite good where we have coverage.

The model parameter uncertainty depends upon the nature of the errors in the data and the data constraints on the model parameters. We shall assume normally distributed errors in the data with rather large uncertainties. In particular, because of the 1 h sampling interval, we specify a standard error of 30 min. The resulting model parameter uncertainty is plotted in Figure 17. Generally, the standard errors are of the order of 0.5 or less where we have good resolution. This is smaller in magnitude than the peak perturbations plotted in Figure 14. However, the error is significant and should improve with better temporal sampling. The error estimates are not accurate where there is no resolution.

4. Discussion and Conclusions

Trajectory-based methods for modeling flow and transport have a long history in hydrology. For example, streamline methods have been used for decades [*Bear*, 1972; *Datta-Gupta and King*, 2007; *Crane and Blunt*, 1999]. As discussed in this paper, the asymptotic approach provides a physical, and corresponding mathematical, basis for trajectory-based modeling. The formulation enables one to connect problems in fluid flow and transport to a diverse range of applications such as quantum mechanics [*Maslov and Fedoryuk*, 1981], gas dynamics [*Anile et al*., 1993], and poroelastic modeling [*Vasco*, 2009]. Hence, methods which are successful in one or more of these areas may be applied to fluid flow and transport modeling.

One area in which asymptotic and trajectory-based methods have proven extremely useful is in the solution of the inverse problem. In particular, using trajectory-based expressions, one can devise an iterative inversion algorithm in which only one steady state pressure simulation is required per iteration step [*Vasco and Datta-Gupta*, 1999]. Such efficiency is critical for developing practical two and three-dimensional inversion schemes [*Datta-Gupta et al*., 2002]. The partitioning of the solution into phase and amplitude terms introduces additional flexibility into the solution of the inverse problem. For example, it allows for the treatment of tracer arrival times in a very efficient fashion, as illustrated here. Travel time or onset times are useful in estimating flow properties from geophysical or X-ray imaging experiments. Specifically, onset times are frequently more sensitive to flow properties and less sensitive to the details of the rock physics model that is used to compute the magnitude of a geophysical response [*Vasco et al*., 2014, 2015]. The partitioning of the solution into phase and amplitude terms also allows for different formulations in setting up the asymptotic expansion and solution. For example, in *Vasco and Finsterle* [2004], the quadratic term due to dispersion appeared in the expression for the amplitude term rather than in the equation for the phase.

Appendix A: An Asymptotic Solution for Dispersive Transport

The underlying idea, motivating the asymptotic approach, is a difference between the length scale of the heterogeneity and the length scale of a propagating tracer front. In particular, the lateral variation of flow properties is assumed to be smoother than the spatial variation of concentration across the tracer front. The length scale associated with the tracer front is defined as the distance over which the tracer concentration changes from the initial background value to a value characteristic of the concentration within the tracer plume. To quantify this, we introduce a length scale L, representing the spatial variation of flow properties such as the hydraulic conductivity tensor $\mathbf{K}$. Similarly, there is a parameter l, corresponding to the length scale over which the concentration varies significantly across a tracer front. I assume that $l \ll L$, and hence the ratio $\epsilon = l/L \ll 1$. One may then define variables, in both space ($\mathbf{X}$) and time (T), in terms of the scale parameter ϵ

$$X_i = \epsilon x_i. \tag{A1}$$

Note that, this approach still allows for discontinuous spatial changes in properties, such as those associated with layering. Such variations are treated as boundary conditions and conditions for reflection and refraction are developed. This treatment is identical to that used for ray methods in the presence of layering and boundaries [*Chapman*, 2004].

Formally, an asymptotic solution of equation (7), which we repeat here for convenience:

$$\nabla \cdot (\mathbf{D} \cdot \nabla C - \mathbf{q}C) - i\omega\varphi_k C = 0, \tag{A2}$$

is a power series expansion in terms of the scale parameter

$$C(\mathbf{x}, \omega, \theta) = e^{\theta(\mathbf{X},\omega)} \sum_{n=0}^{\infty} \epsilon^n C_n(\mathbf{X}, \omega). \tag{A3}$$

The local phase θ is a rapidly varying quantity that has a physical interpretation in terms of a locally propagating front [*Kline and Kay*, 1979].

Note that the partial derivative operators in (A2) may be represented in terms of derivatives with respect to the variables $\mathbf{X}$ and the phase θ. Hence, the for the spatial derivative, contained in the gradient operator, is given as

$$\frac{\partial C}{\partial x_i} = \epsilon \frac{\partial C}{\partial X_i} + \frac{\partial \theta}{\partial x_i}\frac{\partial C}{\partial \theta}. \tag{A4}$$

Higher-order spatial derivatives are obtained by successive applications of (A4).

If we write equation (A2) in terms of $C(\mathbf{X}, \omega)$ and derivatives with respect to X_i, and θ, the following expression results

$$\begin{aligned} &\epsilon^2 \nabla \cdot (\mathbf{D} \cdot \nabla C) \\ &+\epsilon \left[\nabla \cdot (\mathbf{D} \cdot \nabla\theta \frac{\partial C}{\partial \theta}) + \nabla\theta \cdot (\mathbf{D} \cdot \nabla \frac{\partial C}{\partial \theta}) - \nabla \cdot (C\mathbf{q}) \right] \\ &+\nabla\theta \cdot \mathbf{D} \cdot \nabla\theta \frac{\partial^2 C}{\partial \theta^2} - \nabla\theta \cdot \mathbf{q}\frac{\partial C}{\partial \theta} - i\omega\varphi_k C = 0. \end{aligned} \tag{A5}$$

Because of the solution is taken to have the form (A3), the partial derivatives with respect to θ return the original function:

$$\frac{\partial C}{\partial \theta} = \frac{\partial^2 C}{\partial \theta^2} = C,$$

and equation (A5) takes the somewhat simpler form

$$\begin{aligned} &\epsilon^2 \nabla \cdot (\mathbf{D} \cdot \nabla C) \\ &+\epsilon [\nabla \cdot (\mathbf{D} \cdot \nabla\theta C) + \nabla\theta \cdot (\mathbf{D} \cdot \nabla C) - \nabla \cdot (C\mathbf{q})] \\ &+\nabla\theta \cdot \mathbf{D} \cdot \nabla\theta C - \nabla\theta \cdot \mathbf{q}C + i\omega\varphi_k C = 0. \end{aligned} \tag{A6}$$

Substituting the power series expansion (A3) for $C(\mathbf{X}, \omega)$ into (A6) produces an equation with an infinite number of terms of varying orders in ϵ. Because $\epsilon \ll 1$, the most significant terms are associated with the lowest orders of ϵ. In the next two subsections, we examine terms of order ϵ^0 and ϵ^1.

A1. Terms of Order $\epsilon^0 \sim 1$: An Equation for the Phase θ

Retaining only the zeroth order terms in ϵ in equation (A6), after substituting in the power series expansion (A3), results in the expression:

$$[\nabla\theta \cdot \mathbf{D} \cdot \nabla\theta - \nabla\theta \cdot \mathbf{q} + i\omega\varphi_k] C_0 = 0, \tag{A7}$$

where we have factored out the exponential term e^{θ}. Assuming that $C_0(\mathbf{X}, \omega)$ is not identically zero, the quantity in brackets must vanish in order for this equation to be satisfied. Thus, one arrives at the following condition

$$\nabla\theta \cdot \mathbf{D} \cdot \nabla\theta - \nabla\theta \cdot \mathbf{q} + i\omega\varphi_k = 0, \tag{A8}$$

representing a Hamilton-Jacobi equation for $\theta(\mathbf{x}, \omega)$ [*Sneddon*, 2006, p. 81]. Specifically, equation (A8) is a scalar nonlinear, first-order, partial differential equation in which the dependent variable $\theta(\mathbf{x}, \omega)$ is absent. It can be solved numerically, using a technique such as finite differences [*Sethian*, 1999; *Osher and Fedkiw*, 2003, p. 47]. In Appendix B, we adopt the method of characteristics, a well-established approach for solving partial differential equations of the first-order [*Courant and Hilbert*, 1962, p. 62]. Before applying this technique, some simplifications will prove helpful. First, represent the gradient of $\theta(\mathbf{x}, \omega)$ by the phase vector

$$\mathbf{p} = \nabla\theta. \tag{A9}$$

Casting equation (A8) in terms of **p** results in the equation

$$\mathbf{p} \cdot \mathbf{D} \cdot \mathbf{p} - \mathbf{p} \cdot \mathbf{q} + i\omega\varphi_k = 0. \tag{A10}$$

A2. Terms of Order ϵ: An Equation for the Amplitude C_0

Now consider terms of the next lowest order in ϵ in equation (A6). Neglecting terms that must be of order ε^2 or higher produces the equation

$$\begin{aligned} &\varepsilon[\nabla \cdot (\mathbf{D} \cdot \nabla\theta C) + \nabla\theta \cdot (\mathbf{D} \cdot \nabla C) - \nabla \cdot (C\mathbf{q})] \\ &+ [\nabla\theta \cdot \mathbf{D} \cdot \nabla\theta - \nabla\theta \cdot \mathbf{q} + i\omega\varphi_k]C = 0. \end{aligned} \tag{A11}$$

Because of equation (A8), the terms in the last line of equation (A11) vanish and one is left with

$$\nabla \cdot (\mathbf{D} \cdot \mathbf{p}C) + \mathbf{p} \cdot \mathbf{D} \cdot \nabla C - \nabla \cdot (C\mathbf{q}) = 0, \tag{A12}$$

after using the definition (A9). Substituting the asymptotic series (A3) into equation (A12), and neglecting terms of order ε^2 and higher, results in a linear, scalar partial differential equation for $C_0(\mathbf{x}, \omega)$. Expanding the derivatives in that equation and collecting like terms, we can write that differential equation as

$$\Upsilon \cdot \nabla \ln C_0 = \upsilon, \tag{A13}$$

where we have defined the vector coefficient

$$\Upsilon = \mathbf{D} \cdot \mathbf{p} + \mathbf{p} \cdot \mathbf{D} - \mathbf{q} \tag{A14}$$

and the scalar quantity

$$\upsilon = \nabla \cdot (\mathbf{D} \cdot \mathbf{p}) + 2(\mathbf{D} \cdot \mathbf{p}) \cdot \mathbf{p} - \mathbf{p} \cdot \mathbf{q} - \nabla \cdot \mathbf{q}. \tag{A15}$$

Appendix B: Hamilton-Jacobi Equations, the Method of Characteristics, and Trajectories

Following *Courant and Hilbert* [1962, p. 106] and *Sneddon* [2006, p. 81], we write equation (10) in Hamilton-Jacobi form

$$i\omega + H(\mathbf{x}, \mathbf{p}) = 0 \tag{B1}$$

where

$$H(\mathbf{x}, \mathbf{p}) = p_i \frac{D_{ij}}{\varphi} p_j - \frac{q_i}{\varphi_k} p_i, \tag{B2}$$

is the Hamiltonian function. The Hamiltonian is written in index form with the Einstein convention of summation over repeated indices, where the indices run from 1 to 3. Equation (B1) may be treated using the method of characteristics, where the independent variables **x** and **p** are considered to be functions of a scalar quantity *s*. The scalar *s* is a parameter signifying position along a trajectory extending from the source to the observation point. Thus, the independent variables are the coordinates of a trajectory **x**(s), and

$$\mathbf{p}(s) = \nabla\theta. \tag{B3}$$

One may consider equation (B1) to be a nonlinear function of these variables

$$F(\mathbf{x},\mathbf{p},\omega)=i\omega+H(\mathbf{x},\mathbf{p})=0. \tag{B4}$$

Because the independent variables, **x** and **p** are considered to ultimately depend upon *s*, one may compute the total derivative of $F(\mathbf{x},\mathbf{p},\omega)$ with respect to *s*,

$$\frac{dF}{ds}=\frac{\partial F}{\partial x_l}\frac{dx_l}{ds}+\frac{\partial F}{\partial p_l}\frac{dp_l}{ds}=0. \tag{B5}$$

Rewriting equation (B5) in terms of $H(\mathbf{x},\mathbf{p})$ produces the expression

$$\frac{\partial H}{\partial x_l}\frac{dx_l}{ds}+\frac{\partial H}{\partial p_l}\frac{dp_l}{ds}=0. \tag{B6}$$

Equation (B6) may be interpreted geometrically as an orthogonality condition of the two vectors, one containing the partial derivatives of *H* with respect to the independent variables **x** and **p**, the other containing the total derivatives of these variables with respect to *s*. The orthogonality holds if the components of the two vectors are related by

$$\frac{dx_l}{ds}=\frac{\partial H}{\partial p_l}$$
$$\frac{dp_l}{ds}=-\frac{\partial H}{\partial x_l}$$

for $l=1, 2, 3$. These equations constitute the characteristic equations, also known as the ray equations, defining trajectories, **x**(s), along which solutions are defined. The position vector defining the trajectory changes as a function of *s*. Now consider our particular characteristic equations, associated with the Hamiltonian $H(\mathbf{x},\mathbf{p})$ given in (B2). For *H* of this form the characteristic equations are

$$\frac{dx_l}{ds}=2\frac{D_{lj}}{\varphi_k}p_j-\frac{q_l}{\varphi_k},$$
$$\frac{dp_l}{ds}=-p_i\frac{\partial}{\partial x_l}\left(\frac{D_{ij}}{\varphi_k}\right)p_j+\frac{\partial}{\partial x_l}\left(\frac{q_i}{\varphi_k}\right)p_i.$$

We can also write these equations in matrix-vector form:

$$\frac{d\mathbf{x}}{ds}=2\frac{\mathbf{D}}{\varphi_k}\mathbf{p}-\frac{\mathbf{q}}{\varphi_k}$$
$$\frac{d\mathbf{p}}{ds}=-\mathbf{p}^T\cdot\nabla\left(\frac{\mathbf{D}}{\varphi_k}\right)\mathbf{p}+\nabla\left(\frac{\mathbf{q}}{\varphi_k}\right)\cdot\mathbf{p}.$$

The trajectories may be found by integrating this system of ordinary differential equations for the path **x**(s) and the components of the phase gradient **p**(s).

Appendix C: Reduction of the Hamilton-Jacobi Equation to a Scalar Equation for *p*

In this Appendix C, the equation for the phase $\theta(\mathbf{x},\omega)$,

$$\mathbf{p}\cdot\mathbf{D}\mathbf{p}-\mathbf{q}\cdot\mathbf{p}+i\omega\varphi_k=0, \tag{C1}$$

equation (10), will be reduced to a quadratic equation for $p=|\mathbf{p}|$. Such an equation can be factored to produce an analytic expression for *p*. The matrix **D** is real and positive definite but, as noted in the Methodology section, it may not be a symmetric matrix. As such, the matrix has the decomposition

$$\mathbf{D}=\mathbf{U}\mathbf{\Lambda}\mathbf{V}^T \tag{C2}$$

where **U** and **V** are orthogonal matrices, with column vectors given by

$$\mathbf{D}\cdot\mathbf{v}_i=\lambda_i\mathbf{u}_i \tag{C3a}$$
$$\mathbf{D}^T\cdot\mathbf{u}_i=\lambda_i\mathbf{v}_i \tag{C3b}$$

[*Noble and Daniel*, 1977, p. 306], and $\mathbf{\Lambda}$ is a diagonal matrix with entries λ_i. The eigenvalues and vectors may be found from these equations, written in the form

$$\begin{bmatrix} \mathbf{D} & -\lambda_i \mathbf{I} \\ -\lambda_i \mathbf{I} & \mathbf{D}^T \end{bmatrix} \begin{bmatrix} \mathbf{v}_i \\ \mathbf{u}_i \end{bmatrix} = \mathbf{0} \tag{C4}$$

The singular values are found from the condition that the above system of equations has a nonsingular (nonzero) solution. This condition is that the determinant of the coefficient matrix vanishes, resulting in a polynomial equation for λ_i with coefficients that depend upon the elements of the dispersion matrix **D**.

Physically, the structure of the diagonal matrix $\mathbf{\Lambda}$ is related to the interplay between the medium properties and flow-induced anisotropic dispersion. That is, even when the medium has isotropic dispersive properties, the dispersion has been found to be different in the longitudinal direction (in the direction of **q)** and the transverse direction (in directions perpendicular to **q**). For a general anisotropic medium, Λ will contain three distinct scalars, say D_1, D_2, and D_3 along the diagonal. The columns of **U** and **V** are the orthonormal vectors. For a general anisotropic matrix **D**, these vectors might differ from the flow direction. One can denote the two sets of vectors by $\hat{\mathbf{u}}_i$ and $\hat{\mathbf{v}}_i$ where $i = 1, 2, 3$. Thus, **U** is given by

$$\mathbf{U} = [\,\hat{\mathbf{u}}_1 \quad \hat{\mathbf{u}}_2 \quad \hat{\mathbf{u}}_3\,], \tag{C5}$$

and $\mathbf{V}^T$ by

$$\mathbf{V}^T = \begin{bmatrix} \hat{\mathbf{v}}_1^T \\ \hat{\mathbf{v}}_2^T \\ \hat{\mathbf{v}}_3^T \end{bmatrix}. \tag{C6}$$

Now consider the first term in equation (C1)

$$\mathbf{p} \cdot \mathbf{Dp} = \mathbf{p} \cdot \mathbf{U\Lambda V}^T \mathbf{p} \tag{C7}$$

which may be written in terms of the explicit forms (C5) and (C6)

$$\mathbf{p} \cdot \mathbf{Dp} = [\,\mathbf{p} \cdot \hat{\mathbf{u}}_1 \quad \mathbf{p} \cdot \hat{\mathbf{u}}_2 \quad \mathbf{p} \cdot \hat{\mathbf{u}}_3\,] \mathbf{\Lambda} \begin{bmatrix} \mathbf{p} \cdot \hat{\mathbf{v}}_1 \\ \mathbf{p} \cdot \hat{\mathbf{v}}_2 \\ \mathbf{p} \cdot \hat{\mathbf{v}}_3 \end{bmatrix}. \tag{C8}$$

Carry out all of the multiplications in (C8) gives the full expression for the product

$$\mathbf{p} \cdot \mathbf{Dp} = \sum_{i=1}^{3} D_i (\mathbf{p} \cdot \hat{\mathbf{u}}_i)(\mathbf{p} \cdot \mathbf{v}_i) \tag{C9}$$

Because the vectors $\hat{\mathbf{u}}_i$ and $\hat{\mathbf{v}}_i$ are unit vectors, expression (C9) may be written as

$$\mathbf{p} \cdot \mathbf{Dp} = \left[\sum_{i=1}^{3} D_i \cos \mu_i \cos \nu_i \right] p^2, \tag{C10}$$

where

$$\cos \mu_i = \hat{\mathbf{p}} \cdot \hat{\mathbf{u}}_i \tag{C11}$$

and

$$\cos \nu_i = \hat{\mathbf{p}} \cdot \hat{\mathbf{v}}_i \tag{C12}$$

for $i = 1, 2, 3$, the angles between **p** and $\mathbf{u}_i$ and $\mathbf{v}_i$. The expression (C10) may be written in the abbreviated form

$$\mathbf{p} \cdot \mathbf{Dp} = \beta p^2 \tag{C13}$$

where we have defined

$$\beta=\sum_{i=1}^{3} D_i \cos\mu_i \cos\nu_i. \tag{C14}$$

Thus, equation (C1) may be written

$$\beta p^2-\mathbf{q}\cdot\mathbf{p}+i\omega\varphi_k=0, \tag{C15}$$

or as a quadratic equation for p

$$\beta p^2-\gamma p+i\omega\varphi_k=0, \tag{C16}$$

if we define

$$\gamma=q\cos\eta \tag{C17}$$

where $q=|\mathbf{q}|$ and η is the angle between the vectors $\mathbf{p}$ and $\mathbf{q}$.

Acknowledgments
This material is based upon work supported by the U. S. Department of Energy, Office of Science, Office of Basic Energy Sciences, Chemical Sciences, Geosciences, and Biosciences Division under contract DE-AC02-05CH11231. The X-ray data are available upon request from the corresponding author.

References

Anile, A. M., J. K. Hunter, P. Pantano, and G. Russo (1993), *Ray Methods for Nonlinear Waves in Fluids and Plasmas*, Longman, Essex.
Attinger, S., I., Neuweiler, and W. Kinzelback (2001), Macrodispersion in a radially diverging flow field with finite Peclet numbers 2. Homogenization theory approach, *Water Resour. Res.*, *37*, 495–505.
Auriault, J.-L., C. Moyne, and H. P. Amaral Souto (2010), On the asymmetry of the dispersion tensor in porous media, *Transp. Porous Media*, *85*, 771–783.
Bear, J. (1961), On the tensor form of dispersion in porous media, *J. Geophys. Res.*, *66*, 1185–1197.
Bear, J. (1972), *Dynamics of Fluids in Porous Media*, Dover, N. Y.
Blunt, M., K. Liu, and M. R. Thiele (1996), A generalized streamline method to predict reservoir flow, *Pet. Geosci.*, *2*(3), 259–269.
Bracewell, R. N. (1978), *The Fourier Transform and its Applications*, McGraw-Hill, N. Y.
Bratvedt, F., T. Gimse, and C. Tegnander (1996), Streamline computations for porous media flow including gravity, *Transp. Porous Media*, *25*, 63–78.
Bruining, H., M. Darwish, and A. Rijnks (2012), Computation of the longitudinal and transverse dispersion coefficient in an adsorbing porous medium using homogenization, *Transp. Porous Media*, *91*, 833–859.
Carbonell, H. B. G., and S. Whitaker (1983), Dispersion in pulsed systems - II Theoretical developments for passive dispersion in porous media, *Chem. Eng. Sci.*, *38*, 1795–1802.
Chapman, C. H. (2004), *Fundamentals of Seismic Wave Propagation*, Cambridge Univ. Press, Cambridge, U. K.
Chapman, S. J., J. M. H. Lawry, and J. R. Ockendon (1999), Ray theory for high-Peclet-number convection-diffusion, *SIAM J. Appl. Math.*, *60*, 121–135.
Chen, J.-S., C.-F. Ni, and C.-P. Liang (2008), Analytical power series solutions to the two-dimensional advection-dispersion equation with distance-dependent dispersivities, *Hydrol. Processes*, *22*, 4670–4678.
Cirpka, O. A., E. O. Frind, and R. Helmig (1999a), Streamline-oriented grid generation for transport modelling in two-dimensional domains including wells, *Adv. Water Resour.*, *22*, 697–710.
Cirpka, O. A., E. O. Frind, and R. Helmig (1999b), Numerical methods for reactive transport on rectangular and streamline-oriented grids, *Adv. Water Resour.*, *22*, 711–728.
Cleary, R. W., and M. J. Ungs (1978), Groundwater pollution and hydrology, mathematical models and computer programs, *Rep. 78-WR-15*, Water Resour. Program, Princeton Univ., Princeton, N. J.
Cotta, R. M. (1992), *Integral Transforms in Computational Heat and Fluid Flow*, CRC Press, Boca Raton, Fla.
Cotta, R. M., and M. D. Mikhailov (1993), Integral transform method, *Appl. Math. Modell.*, *17*, 156–161.
Courant, R., and D. Hilbert (1962), *Methods of Mathematical Physics*, Interscience, N. Y.
Crane, M. J. and M. J. Blunt (1999), Streamline-based simulation of solute transport, *Water Resour. Res.*, *35*, 3061–3078.
Dagan, G. (1982), Stochastic modeling of groundwater flow by unconditional and conditional probabilities, 2, The solute transport, *Water Resour. Res.*, *18*, 835–848.
Datta-Gupta, A., and M. J. King (1995), A semianalytic approach to tracer flow modeling in heterogeneous permeable media, *Adv. Water Resour.*, *18*, 9–24.
Datta-Gupta, A., and M. J. King (2007), *Streamline Simulation: Theory and Practice*, Soc. of Pet. Eng., Richardson, Tex.
Datta-Gupta, A., S. Yoon, D. W. Vasco, and G. A. Pope (2002), Inverse modeling of partitioning interwell tracer tests: A streamline approach, *Water Resour. Res.*, *38*(6), 1079, doi:10.1029/2001WR000597.
de Josselin de Jong, G. (1958), Longitudinal and transverse diffusion in granular deposits, *Trans. AGU*, *39*, 67–74.
de Marsily, G. (1986). *Quantitative Hydrogeology*, Academic, San Diego, Calif.
Didierjean, S., H. P. Amaral Souto, R. Delannay, and C. Moyne (1997), Dispersion in periodic porous media, experience versus theory for two-dimensional systems, *Chem. Eng. Sci.*, *52*, 1861–1874.
Fel, L., and J. Bear, (2010), Dispersion and dispersivity tensors in saturated porous media with uniaxial symmetry, *Transp. Porous Media*, *85*, 259–268.
Flekkoy, E. G. (1993), Lattice Bhatnagar-Gross-Krook models for miscible fluids, *Phys. Rev. E*, *47*, 4247–4257.
Gardner, C. S., and G. K. Morikawa (1960), *Similarity in the asymptotic behavior of collision-free hydromagnetic waves and water waves*, Report 9082, pp. 1–30, Courant Institute of Mathematical Sciences, N. Y.
Gelhar, L. W., and C. L. Axness, (1983), Three-dimensional stochastic analysis of macrodispersion in aquifers *Water Resour. Res.*, *19*, 161–180.
Gelhar, L. W., and M. A. Collins (1971), General analysis of longitudinal dispersion in nonuniform flow, *Water Resour. Res.*, *7*, 1511–1521.
Gelhar, L. W., A. L. Gutjahr, and R. L. Naff (1979), Stochastic analysis of macrodispersion in a stratified aquifer, *Water Resour. Res.*, *15*, 1387–1397.

Guerrero, J. S. P., and T. H. Skaggs (2010), Analytical solution for one-dimensional advection-diffusion transport with distance-dependent coefficients, *J. Hydrol.*, *390*, 57–65.
Hornung, U. (1997), *Homogenization and Porous Media, Interdisciplinary Applied Mathematics*, vol. 6, Springer, Berlin, doi:10.1007/978-1-4612-1920-0.
Javandel, I., C. Doughty, and C. F. Tsang (1984), *Groundwater Transport: Handbook of Models*, AGU, Washington, D. C.
Kline, M., and I. W. Kay (1979), *Electromagnetic Theory and Geometrical Optics*, Robert E. Krieger Publ. Co., Huntington, N. Y.
Knessl, C., and J. B. Keller (1997), Advection-diffusion past a strip. II. Oblique incidence, *J. Math. Phys.*, *38*, 267–282.
Koch, D. L., and J. F. Brady (1987), The symmetry properties of the effective diffusivity tensor in anisotropic porous media, *Phys. Fluids*, *30*, 642–650.
Kravtsov, Y. A., and Y. I. Orlov (1990), *Geometrical Optics of Inhomogeneous Media*, Springer, Berlin.
Liu, Y., and P. K. Kitanidis (2013), A mathematical and computational study of the dispersivity tensor in anisotropic media, *Adv. Water Resour.*, *62*, 303–316.
Liu, Y., and B. C. Si (2008), Analytic modeling of one-dimensional diffusion in layered systems with position-dependent diffusion coefficients, *Adv. Water Resour.*, *31*, 251–268.
Maslov, V. P., and M. V. Fedoryuk (1981), *Semi-Classical Approximation in Quantum Mechanics*, D Reidel, Hingham, Mass.
Mikhailov, M. D., and M. N. Özisik (1984), *Unified Analysis and Solutions of Head and Mass Diffusion*, John Wiley, N. Y.
Moridis, G. J. (2002), Semianalytical solutions of radioactive or reactive solute transport in a variably fractured layered media, *Water Resour. Res.*, *38*(12), 1310, doi:10.1029/2001WR001028.
Nikolaevskii, V. N. (1959), Konvektivnaya diffusiya v poristykh sredakh, *Prikl. Mat. Mekh.*, *23*(6), 1042–1050.
Noble, B., and J. W. Daniel (1977), *Applied Linear Algebra*, Prentice Hall, Englewood Cliffs, N. J.
Oldenburg, C. M., and K. Pruess (1993), A two-dimensional dispersion module for the TOUGH2 simulator, *Rep. 78-WR-15*, Earths Sci. Div., Lawrence Berkeley Lab., Berkeley, Calif.
Oldenburg, C. M., and K. Pruess (1995), Dispersive transport dynamics in a strongly coupled groundwater-brine flow system, *Water Resour. Res.*, *31*, 289–302.
Oldenburg, C. M., and K. Pruess (1996), Mixing with first-order decay in variable-velocity porous media flow, *Transp. Porous Media*, *22*, 161–180.
Osher, S., and R. Fedkiw (2003), *Level Set Methods and Dynamic Implicit Surfaces*, Springer, N. Y.
Paige, C. C., and M. A. Saunders (1982), LSQR: An algorithm for sparse linear equations and sparse linear systems, *ACM Trans. Math. Software*, *8*, 195–209.
Park, E., and H. Zhan (2001), Analytical solutions of contaminant transport from finite one-, two-, and three-dimensional sources in a finite-thickness aquifer, *J. Contam. Hydrol.*, *53*, 41–61.
Parker, R. L. (1994), *Geophysical Inverse Theory*, Princeton Univ. Press, Princeton, N. J.
Press, W. H., S. A. Teukolsky, W. T. Vetterling, and B. P. Flannery (1992), *Numerical Recipes*, Cambridge Univ. Press, Cambridge, U. K.
Pruess, K., C. Oldenburg, and G. Moridis (1999), *TOUGH2 User's Guide, Version 2.0*, *LBNL Rep. 43134*, Lawrence Berkeley Nat. Lab., Berkeley, Calif.
Saffman, P. G. (1959), A theory of dispersion in porous media, *J. Fluid Mech.*, *6*, 321–349.
Sahimi, M. (1993), Flow phenomena in rocks: From continuum models to fractals, percolation, cellular automata, and simulated annealing, *Rev. Modern Phys.*, *65*, 1393–1534.
Sassiat, P. R., P. Mourier, M. H. Caude, and R. H. Rosset (1987), Measurement of diffusion coefficients in supercritical carbon dioxide and correlation with the equation of Wilke and Chang, *Anal. Chem.*, *59*, 1164–1170.
Scheidegger, A. E. (1954), Statistical hydrodynamics in porous media, *J. Appl. Phys.*, *25*, 894–1001.
Scheidegger, A. E. (1961), General theory of dispersion in porous media, *J. Geophys. Res.*, *66*, 3273–3278.
Schwartz, F. W. (1977), Macroscopic dispersion in porous media: The controlling factors, *Water Resour. Res.*, *13*, 743–752.
Sethian, J. A. (1999), *Level Set Methods*, Cambridge Univ. Press, Cambridge, U. K.
Shan, C., and I. Javandel (1997), Analytical solutions for solute transport in a vertical aquifer section, *J. Contam. Hydrol.*, *27*, 63–82.
Sim, Y., and C. V. Chrysikopoulos (1999), Analytical solutions for solute transport in saturated porous media with semi-infinite or finite thickness, *Adv. Water Resour.*, *22*, 507–519.
Smith, R. (1981), The early stages of contaminant dispersion in shear flows, *J. Fluid Mech.*, *111*, 107–122.
Sneddon, I. N. (2006), *Elements of Partial Differential Equations*, Dover, N. Y.
Su, N., G. C. Sander, F. Liu, V. Anh, and D. A. Barry (2005) Similarity solutions for solute transport in fractal porous media with time- and scale-dependent dispersivity, *Appl. Math. Modell.*, *29*, 852–870.
Taylor, G. (1953), Dispersion of soluble matter in solvent flowing slowly through a tube, *Proc. R. Soc. London, Ser. A*, *219*, 186–203.
Taylor, G. (1954), Conditions under which dispersion of a solute in a stream of solvent can be use to measure molecular diffusion, *Proc. R. Soc. London, Ser. A*, *225*, 473–477.
van Genuchten, M., and W. J. Alves (1982), Analytical solutions of the one-dimensional convective-dispersion solute transport equation, *U.S.D.A. Tech. Bull.*, *1661*, 1–151.
Vasco, D. W. (2009), Modelling broad-band poroelastic propagation using an asymptotic approach, *Geophys. J. Int.*, *179*, 299–318.
Vasco, D. W., and A. Datta-Gupta (1999), Asymptotic solutions for solute transport: A formalism for tracer tomography, *Water Resour. Res.*, *35*, 1–16.
Vasco, D. W., and S. Finsterle (2004), Numerical trajectory calculations for the efficient inversion of flow and tracer observations, *Water Resour. Res.*, *40*, W01507, doi:10.1029/2003WR002362.
Vasco, D. W., A. Datta-Gupta, and J. C. S. Long (1997), Resolution and uncertainty in hydrologic characterization, *Water Resour. Res.*, *33*, 379–397.
Vasco, D. W., H. Keers, and K. Karasaki (2000), Estimation of reservoir properties using transient pressure data: An asymptotic approach, *Water Resour. Res.*, *36*, 3447–3465.
Vasco, D. W., T. M. Daley, and A. Bakulin (2014), Utilizing the onset of time-lapse changes: A robust basis for reservoir monitoring and characterization, *Geophys. J. Int.*, *197*, 542–556, doi:10.1093/gji/ggt526.
Vasco, D. W., A. Bakulin, H. Baek, and L. R. Johnson (2015), Reservoir characterization based upon the onset of time-lapse amplitude changes, *Geophysics*, *80*, M1–M14, doi:10.1190/GEO2014-0076.1.
Virieux, J., C. Flores-Luna, and D. Gibert, (1994), Asymptotic theory for diffusive electromagnetic imaging, *Geophys. J. Int.*, *119*, 857–868.
Warren, J. E., and F. F. Skiba (1964), Macroscopic dispersion, *Trans. Am. Inst. Min. Metall. Pet. Eng.*, *231*, 215–230.
Xu, L., and M. L. Brusseau (1996), Semianalytical solution for solute transport in porous media with multiple spatially variable reaction processes, *Water Resour. Res.*, *32*, 1985–1991.

Yabusaki, S. B., C. I. Steefel, and B. D. Wood (1998), Multidimensional, multicomponent, subsurface reactive transport in nonuniform velocity fields: Code verification using an advective reactive streamtube approach, *J. Contam. Hydrol.*, *30*, 299–331.

Yates, S. R. (1990), An analytical solution for one-dimensional transport in heterogeneous porous media, *Water Resour. Res.*, *26*, 2331–2338.

Zoppou, C., and J. H. Knight (1999), Analytical solution of a spatially variable coefficient advection-diffusion equation in up to three dimensions, *Appl. Math. Modell.*, *23*, 667–685.